



Research Article

Local endothelial DNA repair deficiency causes aging-resembling endothelial-specific dysfunction

Paula K. Bautista-Niño^{1,2,*}, Eliana Portilla-Fernandez^{1,3,*}, Eloisa Rubio-Beltrán¹, Janette J. van der Linden^{1,6}, René de Vries¹, Richard van Veghel¹, Martine de Boer⁴, Matej Durik^{1,5}, Yanto Ridwan^{6,7}, Renata Brandt⁶, Jeroen Essers^{6,7,8}, Robert I. Menzies⁹, Rachel Thomas¹⁰, Alain de Bruin¹⁰, Dirk J. Duncker⁴, Heleen M.M. van Beusekom⁴, Mohsen Ghanbari³, Jan H.J. Hoeijmakers^{6,11,12}, Radislav Sedlacek¹³,  Rhian M. Touyz¹⁴, Augusto C. Montezano¹⁴, Ingrid van der Pluijm^{6,8}, A.H. Jan Danser¹, Kristian A. Haanes^{1,15} and  Anton J.M. Roks¹

¹Division of Vascular Medicine and Pharmacology, Department of Internal Medicine, Erasmus University Medical Center, Rotterdam, The Netherlands; ²Fundacion Cardiovascular de Colombia FCV, Dept. of Cardiology, Bucaramanga, Colombia; ³Department of Epidemiology, Erasmus University Medical Center, Rotterdam, The Netherlands; ⁴Division of Experimental Cardiology, Department of Cardiology, Thoraxcenter, Erasmus University Medical Center, Rotterdam, The Netherlands; ⁵Department of Pediatric and Adolescent Medicine, Mayo Clinic College of Medicine, Rochester, MN, U.S.A.; ⁶Department of Molecular Genetics, Erasmus University Medical Center, Rotterdam, The Netherlands; ⁷Department of Radiology and Nuclear Medicine, Erasmus University Medical Center, Rotterdam, The Netherlands; ⁸Department of Vascular Surgery, Erasmus University Medical Center, Rotterdam, The Netherlands; ⁹Centre for Cardiovascular Science, The University of Edinburgh, Edinburgh, U.K.; ¹⁰Dutch Molecular Pathology Centre, Faculty of Veterinary Medicine, Department of Pathobiology, Utrecht University, Utrecht, The Netherlands; ¹¹CECAD Forschungszentrum, Universität zu Köln, Cologne, Germany; ¹²Princess Máxima Center for Pediatric Oncology, ONCODE Institute, Utrecht, The Netherlands; ¹³Laboratory of Transgenic Models of Diseases and Czech Centre for Phenogenomics, Institute of Molecular Genetics of the ASCR, Prague, Czech Republic; ¹⁴Institute of Cardiovascular and Medical Sciences, University of Glasgow, Glasgow, U.K.; ¹⁵Department of Clinical Experimental Research, Glostrup Research Institute, Copenhagen University Hospital, Copenhagen, Denmark

Correspondence: Anton J.M. Roks (a.roks@erasmusmc.nl)

We previously identified genomic instability as a causative factor for vascular aging. In the present study, we determined which vascular aging outcomes are due to local endothelial DNA damage, which was accomplished by genetic removal of ERCC1 (excision repair cross-complementation group 1) DNA repair in mice (EC-knockout (EC-KO) mice). EC-KO showed a progressive decrease in microvascular dilation of the skin, increased microvascular leakage in the kidney, decreased lung perfusion, and increased aortic stiffness compared with wild-type (WT). EC-KO showed expression of DNA damage and potential senescence marker p21 exclusively in the endothelium, as demonstrated in aorta. Also the kidney showed p21-positive cells. Vasodilator responses measured in organ baths were decreased in aorta, iliac and coronary artery EC-KO compared with WT, of which coronary artery was the earliest to be affected. Nitric oxide-mediated endothelium-dependent vasodilation was abolished in aorta and coronary artery, whereas endothelium-derived hyperpolarization and responses to exogenous nitric oxide (NO) were intact. EC-KO showed increased superoxide production compared with WT, as measured in lung tissue, rich in endothelial cells (ECs). Arterial systolic blood pressure (BP) was increased at 3 months, but normal at 5 months, at which age cardiac output (CO) was decreased. Since no further signs of cardiac dysfunction were detected, this decrease might be an adaptation to prevent an increase in BP. In summary, a selective DNA repair defect in the endothelium produces features of age-related endothelial dysfunction, largely attributed to loss of endothelium-derived NO. Increased superoxide generation might contribute to the observed changes affecting end organ perfusion, as demonstrated in kidney and lung.

*These authors contributed equally to this work.

Received: 21 February 2019

Revised: 21 January 2020

Accepted: 23 March 2020

Accepted Manuscript online:

23 March 2020

Version of Record published:

07 April 2020

Introduction

Despite the currently available prevention and treatment options, cardiovascular diseases (CVDs) continue to be a main cause of morbidity and mortality worldwide. Even when traditional risk factors are absent or controlled, cardiovascular problems remain a major health issue as reflected by the independent risk factor, age [1]. Aging, which is not synonymous to age, is a natural but very complex process leading to the decline and ensuing loss of organ function. The accumulation of DNA damage is considered as one of the primary causes driving the process of aging, and involves various processes [2,3]. First, cells with unrepaired DNA damage may enter into apoptosis or senescence; apoptosis can lead to atrophy and organ function decline due to the loss of cells or tissue, and senescence-related mechanisms trigger the acquisition of a senescence-associated secretory phenotype (SASP) that affects surrounding cells and triggers age-related traits [4]. In parallel, accumulating DNA damage also triggers a so-called ‘survival response’ that switches the organism’s physiological status from one that promotes growth to one that suppresses growth and focuses on maintenance of cellular homeostasis and function [5]. In humans, the presence of individual genetic and environmental variations evoke differences in the rate of aging among individuals, but also between organs within an individual. This differential pace of aging is also observed in mouse models of accelerated aging as provoked by DNA repair defects [5].

Several mouse models have been generated that, by deficiency of specific repair pathways, show striking similarities to human aging [5]. One of these models is the *Ercc1*^{Δ/−} mouse. The Δ allele is a truncation of the Excision Repair Cross-Complementation group 1 (ERCC1) protein by seven amino acids of its C-terminus [6]. This results in a hypomorph mutation, that largely (but not completely) abolishes its interaction with the XPF protein. ERCC1–XPF forms a heterodimeric structure-specific endonuclease that incises the damaged strand at some distance 5′ of the lesion [7]. The Δ allele has approximately 10% residual activity, causing impaired function of the protein, progressive accumulation of DNA damage, and numerous features of accelerated aging, which are strongly delayed by dietary restriction, the only universal anti-aging intervention [8].

ERCC1 is an essential component in the pathway of DNA nucleotide excision repair (NER), which removes a wide class of helix-distorting DNA lesions induced by UV, chemicals, and oxidative stress. Apart from that, ERCC1 is involved in other DNA repair systems such as double-strand break and cross-link repair [9]. Mutations in proteins of the NER pathway have shown severe effects on human health as evidenced in several human progeroid syndromes such as Cockayne syndrome, trichothiodystrophy, and Xpf-Ercc1 syndrome [7,10].

Ercc1^{Δ/−} mice are short-lived (24–28 weeks) and within 12 weeks from birth develop neurodegeneration, osteoporosis, many features of aging in liver, kidney, heart, muscle, and the hematopoietic system. In 8-week-old *Ercc1*^{Δ/−} mice an increased blood pressure (BP) was observed, which appeared to become less apparent at 12 weeks of age [11,12]. Thus, the BP increase might be biphasic. Also, increased vascular stiffness and loss of macro- and microvascular dilator function were observed [11]. The vasodilator dysfunction in *Ercc1*^{Δ/−} mice is explained by reduced NO-cGMP (cyclic guanosine monophosphate) signaling, partly due to decreased endothelial nitric oxide synthase (eNOS) expression [11]. Many of these features are very similar to what was previously found in normal rodent and human aging.

Segmental progeria observed in *Ercc1*^{Δ/−} mice implies that affected organs might be influenced by the impact of local and/or systemic DNA damage, processes associated with oxidative stress. To address the question if a local endothelial DNA repair defect is critical for the specific changes in vascular function as observed in *Ercc1*^{Δ/−} mice, we investigated cardiovascular function in a mouse model with specific loss of *Ercc1* in vascular endothelial cells (ECs).

Methods

Animals

We evaluated the effect of endothelial genomic instability on cardiovascular function in a mouse model with endothelium-specific deletion of *Ercc1* (*Tie2Cre*⁺ *Ercc1*^{fl/fl} mouse model). To target the endothelium, various Cre recombinase models are available. *Tie2Cre* models have been used most widely. VE-Cadherin-(CD144) Cre models have been suggested as being perhaps the models in which the endothelium is targeted most uniformly [13]. However, the only example known to us in which a direct comparison is made between the models does not reveal a difference, at least, when used for fate mapping purposes of EC in adult organs [14]. Both *Tie2* and VE-Cadherin are not only expressed in ECs, but also in hematopoietic (stem) cells (HSCs), potentially affecting leukocyte populations of HSC-derived lineage [15–18]. Interestingly, *Tie2* is known to be expressed in lineages forming monocytes that have a pro-angiogenic function [17]. Thus, leukocytes specifically devoted to endothelial maintenance would be undermined, possibly preventing the recovery of the endothelium if *Ercc1* deletion indeed leads to dysfunction of

the mature endothelium. Therefore, we preferred the *Tie2* promoter region as the sequence driving Cre-recombinase. To explore the consequences of Tie2Cre-driven *Ercc1* deletion in HS,C we have examined the blood of the relevant mouse strains (see below).

The Cre-loxP system was used to generate a conditional mouse model expressing Cre-recombinase under the control of the vascular EC receptor tyrosine kinase (*Tie2*) promoter (Tie2Cre). *Tie2Cre*^{+/-} female mice were crossed with *Ercc1*^{+/-} male mice to generate *Tie2Cre*^{+/-} *Ercc1*^{+/-} mice in a pure C57BL/6J background. The females were then crossed with *Ercc1*^{fl/fl} male mice in a pure FVB/N background to produce *Tie2Cre*⁺ *Ercc1*^{fl/-} mice in a C57BL6/FVB F1 hybrid background [19]. These *Tie2Cre*⁺ *Ercc1*^{fl/-} mice were homozygous for *Ercc1*, after deletion of the floxed allele in ECs expressing Cre-recombinase. These mice are referred throughout this manuscript as EC-knockout mice (EC-KO). Littermates (genotypes: *Tie2Cre*⁺ *Ercc1*^{fl/+}, *Tie2Cre*⁻ *Ercc1*^{fl/+}, *Tie2Cre*⁻ *Ercc1*^{fl/-}) were used as controls. All control mouse genotypes were combined and are referred to as wild-type (WT) mice in the paper. In order to test for potential differences between control genotypes, we performed some analyses separating the *Cre*⁺ *Ercc1*^{fl/+} mice. For reactive hyperemia, *ex vivo* vascular function and mechanical properties of the carotid, we analyzed *Cre*⁺ *Ercc1*^{fl/+} mice as a separate group. Mice were kept in individually ventilated cages, in a 12-h light/dark cycle and fed normal chow and water *ad libitum*.

EC-KO mice unexpectedly died at the age of 5.5–6 months (100% of the cases). Consequently, we decided to evaluate mice at 3 and 5 months of age. Mice under profound anesthesia were killed by exsanguination from the vena porta. All animal procedures were performed at the Erasmus MC facility for animal experiments following the guidelines from Directive 2010/63/EU of the European Parliament on the protection of animals used for scientific purposes. All animal studies were approved by the Animal Care Committee of Erasmus University Medical Center Rotterdam (protocol number 118-13-03).

Pathological examination, tissue collection, and blood analysis

All sudden deaths of EC-KO occurred at night, except for two cases. One of these two mice was submitted to whole body fixation in formalin for 48 h and pathological examination. Tissues were processed by paraffin-embedding techniques, sectioned, and stained with Hematoxylin and Eosin. Slides were examined by a board-certified veterinary pathologist. For mice killed at 3 and 5 months of age, blood was collected under anesthesia from the vena porta and analyzed for cell counts. Vascular, cardiac, renal, and lung tissue were collected for further study. For scanning electron microscopy (EM) abdominal aorta was fixed in 4% formaldehyde/2% glutaraldehyde. The lumen was exposed after longitudinal opening of the aorta, and scanning EM recordings were made after platinum sputtering.

Blood vessel permeability

We performed Evans Blue dye method in mice, as described [20], to determine the presence of vascular leakage in kidneys. In brief, we injected 100 μ l of 1% Evans Blue dye (0.133 g of Evans Blue in 10 ml of PBS with Ca^{2+} and Mg^{2+} , prepared under sterile conditions) through femoral cannulation. After 4 h of incubation, blood was drawn (100–200 μ l). Blood sampling was followed by whole animal PBS perfusion through the femoral infusion cannula after opening of the right atrium. Perfusion was performed with a peristaltic rotation pump until no blood residue remained in the atrium. Kidneys were collected, weighted, and transferred to sample tubes with 500 μ l of formamide. The sample tubes were incubated in a heat block at 55°C for 24 h to extract Evans Blue from the tissue. After incubation, the formamide/Evans Blue mixture was centrifuged to pellet any remaining tissue fragments. Absorbance of each sample was measured at 610 nm (VersaMax™ Microplate Reader). Absorbance values from a standard curve with known concentrations of Evans Blue in formamide, with pure formamide as a background blank, and the total weight of each sample, were used to calculate the amount of Evans Blue per mg of renal tissue.

Cardiac function

Cardiac geometry and function were measured by performing 2-D guided short axis M-mode transthoracic echocardiography (Vevo770 High-Resolution Imaging System, VisualSonics) equipped with a 35-MHz probe. Left ventricular (LV) external and internal diameters were traced, and heart rate, LV mass and fractional shortening were subsequently calculated using the VisualSonics Cardiac Measurements Package. Mice were anesthetized with 2.5% and maintained with 2.0% isoflurane, the animals were breathing freely and intubation was not required, while body temperature was kept at 37°C.

BP measurement

BP was measured non-invasively in conscious mice using the tail cuff technique (CODA High-Throughput device, Kent Scientific). BP was measured on five consecutive days and each session consisted of 30 measurement cycles for each mouse. The first 4 days were taken as acclimatization sessions. BP values reported here correspond to the average of all valid measurements recorded at day 5.

In vivo aortic strain

Using the data on systolic and diastolic aortic diameters acquired by transthoracic echocardiography, we calculated aortic strain by subtracting the diastolic aortic diameter from the systolic aortic diameter.

Microvascular vasodilator function and lung perfusion *in vivo*

We assessed *in vivo* vasodilator function using Laser Doppler perfusion imaging, after 3–7 days of BP measurement. Reactive hyperemia, defined as the increase in the hindleg perfusion after temporary occlusion of the blood flow, was calculated. Blood flow was measured in the left hindleg one day after removing the leg's hair using a hair removal cream. The hindleg was kept still with help of a fixation device. After recording baseline perfusion for 5 min, blood flow was occluded for 2 min with a tourniquet. To record hyperemia and the return of the blood flow to the post-occlusion baseline, blood flow was monitored for 10 min after releasing the tourniquet. During all measurements mice were under 2.8% isoflurane anesthesia, and temperature was constantly monitored and maintained between 36.4 and 37.0°C. For each mouse we calculated the maximum response to occlusion and the area under the curve relative to the post-occlusion baseline. Only the area above the baseline was considered. Values below the baseline were set at 0.

In a separate set of 5 month-old WT vs. EC-KO ($n=4$ vs 7), lung perfusion was measured by microCT imaging. μ CT scans were performed and reconstructed at the Applied Molecular Imaging Erasmus MC facility (AMIEf) by using the Quantum FX (PerkinElmer). Mice were anesthetized with 2.5% isoflurane in O₂ and received an IV injection with eXIA160 (Binitio Biomedical Inc., Canada) contrast agent. The injected amount of agent followed the dose recommended by the manufacturers. First, a pre-contrast scan was made as a baseline. The animal was taped to the imaging bed with a catheter placed in the tail vein to ensure minimal displacement and prevent misalignment during post-processing. After acquisition of the pre-contrast scan, the contrast agent was slowly infused (150–200 μ l in 1 min), after which a second scan was made. Mice were scanned using intrinsic cardio-respiratory gating to reduce artifacts caused by breathing. CT acquisition parameters: 90 kV, 160 μ A, field of view 20 mm, 40 μ m resolution with an acquisition time of 4.5 min. Scans were quantified using Analyze 11.0 software (AnalyzeDirect). By using the image calculator option the pre-contrast image was subtracted from the post-contrast image. This resulted into an image of iodine only, which was subjected to further filtering with a median filter (kernel size: 3 \times 3 \times 3). During semi-automatic segmentation of the lungs, the large and midsize blood vessels were excluded. On the resulting lung image segmentation, we calculated the average intensity value as a measure for average lung perfusion, with a minimum of 40% of total lung volume.

Ex vivo vascular functional assessment

Immediately after killing, thoracic aorta, iliac and left anterior descending coronary arteries were carefully dissected from mice and kept in cold Krebs–Henseleit buffer (in mmol/l: NaCl 118, KCl 4.7, CaCl₂ 2.5, MgSO₄ 1.2, KH₂PO₄ 1.2, NaHCO₃ 25, and glucose 8.3 in distilled water; pH 7.4). Vessel rings of 1.5–2 mm length were mounted in small wire myograph organ baths (Danish Myograph Technology, Aarhus, Denmark) containing 6 ml of Krebs–Henseleit buffer oxygenated with 95% O₂ and 5% CO₂. After warming, the tension was normalized by stretching the vessels in steps until 90% of the estimated diameter at which the effective transmural pressure of 100 mmHg is reached. Thereafter, the viability of the vessels was tested by inducing contractions with 30 and 100 mmol/l KCl. After the maximum response to KCl had been reached vessels were washed. To evaluate vasodilatory responses, aortic and iliac segments were first pre-constricted with 30 nmol/l of the thromboxane A₂ analog U46619, resulting in a precontraction corresponding with 50–100% of the response to 100 mmol/l KCl. After this, concentration–response curves (CRCs) were constructed with the endothelium-dependent vasodilator acetylcholine (ACh) at cumulative doses (10^{−10}–10^{−5} mol/l). When the CRC to ACh was completed, we used the endothelium-independent vasodilator sodium nitroprusside (SNP, 10^{−4} mol/l). Complete CRCs to SNP (10^{−10}–10^{−4} mol/l) were performed in parallel rings precontracted with 30 nmol/l U46619.

The contribution of nitric oxide (NO) and prostaglandins in the aortic ACh responses was explored by performing the experiments in the presence of the NO synthase inhibitor NG-nitro-L-arginine methyl ester salt (L-NAME, 10^{−4}

mol/l) and the cyclo-oxygenase (COX) inhibitor indomethacin (INDO, 10^{-5} mol/l). Inhibitors were added to the organ bath 20 min prior to U46619.

To assess the potential involvement of reactive oxygen species (ROS) in the blunted vasodilator response to ACh, we used N-acetyl-cysteine (NAC; 10^{-2} mol/l), which is an aminothiols and synthetic precursor of intracellular cysteine and GSH and a non-specific ROS scavenger [21]. Moreover to determine whether altered vasodilation involves hydrogen peroxide, we used PEG-catalase (PEG-CAT; 0.01 mg/ μ l), which catalyzes the decomposition of hydrogen peroxide to water and O₂. Vessels were pre-treated with NAC or PEG-CAT for 1 h prior to the ACh dose-response curve.

In coronary arteries we investigated endothelium-dependent vasodilation by performing CRCs to ACh and to the adenosine 5'-O-(2-thiodiphosphate) (ADP β S) and Uridine-5'-O-(3-thiotriphosphate) (UTP γ S). The intracellular signaling activation caused by ADP and UTP, has not been studied in detail in the mouse heart. However, studies on BP and cerebral arterioles in the eNOS^{-/-} mice have shown that the two nucleotides do not cause vasodilation through the same mechanisms. It is thought that UTP-induced vasodilation exclusively involves endothelium-dependent hyperpolarization (EDH) [22], while ADP acts through both NO and EDH on a 50%/50% basis.[23] CRCs to ADP β S and UTP γ S were performed in coronary arteries precontracted with U46619 and then in coronary segments precontracted with 30 mM KCl. The latter was done to elucidate the contribution of EDH in ADP β S- and UTP γ S-induced vasodilation because when arteries are precontracted with 30 mmol/l KCl, EDH cannot occur because the artery is too strongly depolarized [24–26]. Vascular smooth muscle cell (VSMC) dilatory function was tested by constructing CRCs to the NO donor SNP.

In iliac rings, after washing out KCl 100 mmol/l, we investigated contractile responses to angiotensin II (Ang II, 10^{-10} – 10^{-7} mol/l), endothelin-1 (ET-1 10^{-10} – 10^{-6} mol/l) and phenylephrine (PE, 10^{-9} – 10^{-5} mol/l). For detailed information, see Supplementary Methods.

Mechanical properties and dimensions of the vascular wall

Carotid arteries explanted from 5 months old mice were mounted in a pressure myograph (Danish Myograph Technology (DMT), Aarhus, Denmark) in calcium-free buffer (in mmol/l: NaCl 120, KCl 5.9, EGTA 2, MgCl₂ 3.6, NaH₂PO₄ 1.2, glucose 11.4, NaHCO₃ 26.3; pH 7.4). The intraluminal pressure of the carotid artery was increased stepwise by 10 mmHg starting at 0 mmHg and reaching 120 mmHg. Lumen and vessel diameter were measured and used to calculate wall strain and stress [27].

Mechanical properties of the aortic wall were tested in a protocol that was earlier described by Fleenor et al. [28]. In short, aortic segments of 1.5–2.0 mm length were hung in small wire organ baths filled with Ca²⁺-free buffer with clamps just touching each other (zero position). After 1 h of acclimatization the rings were pre-stretched three times for 3 min to 1 mm separation of the clamps from the zero position. After returning again to the zero position, the rings were set to a pretension of 1 mN by moving the clamps apart. The strain at this distance of the two clamps was set at '1'. A series of 10% increasing strain values was created by stepwise increase in the clamp distance, with 3-min pauses between each step for equilibration. Thus, a series of 1, 1.1, 1.2, . . . , 2.5 was constructed. The wires were not able to withstand more tension without bending. Burst point was not reached. Thus, applying this method we were able to measure mechanical properties of the aortic wall in the force range representing the plasticity observed in the physiological BP range (80–120 mmHg; strain of 1.5–2.0, as determined with DMT normalization software), and beyond. For the force developed at each strain (λ) of unidirectional displacement, stress (S) was calculated applying the formula $S = \lambda F/2HL$, with F = developed force in mN, T = wall thickness, L = length of vessel segment. Wall thickness and other variables presented herein were measured by light microscopy, using calibrated Leica QWin software (Germany), at 50 \times magnification in 10 μ m, Eosin-stained cryo-sections made from separately isolated aortic tissue of the area adjacent to the segment tested in the organ bath. Six EC-KO vs. seven WT were tested of which one WT was a statistical outlier for stress at strain 2.4, one WT stiffness measurement failed due to technical problems with the organ bath set up. Only sections of segments that formed a complete vessel wall and that were, by approximation, circular were included for measurement of vessel diameter and circumference, explaining the lower *n* in EC-KO for these measurements.

Quantitative real-time PCR

Total RNA was isolated from aortic tissue and cDNA was prepared, which was amplified by real-time PCR on a StepOne Thermocycler (Applied Biosystems). Each reaction was performed in duplicate with SYBR Green PCR Master Mix (Applied Biosystems). β -actin and HPRT-1 were used for normalization. The relative amount of genomic

DNA in DNA samples was determined as follows: $RQ = 2^{(-\Delta\Delta C_t)}$. Sequences of the primers used are provided in Supplementary Table S1.

Immunoblots and immune histology

Frozen tissues were homogenized in ice-cold RIPA buffer (50 mmol/l HCl pH 7.4, 150 mmol/l NaCl, 1% NP-40, 0.25% Na-deoxycholate and 1 mmol/l EDTA) containing protease and phosphatase inhibitors (1 mmol/l PMSF, 1 mmol/l NaVO₄, 1 mmol/l NaF, 1 µg/ml aprotinin, 1 µg/ml pepstatin and 1 µg/ml leupeptin) using a stainless-steel ultraturrax (Polytron). Homogenized tissues were centrifuged and protein concentration was measured in the supernatants using the BCA method (Thermo Scientific, U.S.A.). Membranes were blocked with 3–5% milk or 5% BSA in TBS-T. After blocking, membranes were incubated overnight with the primary antibodies as follows: eNOS (Santa Cruz, SC-654 1:500 in 5% milk TBS-T), pSer¹¹⁷⁷-eNOS (Santa Cruz, SC-21871-R 1:500 in 5% BSA TBS-T), and Ercc1 (Abcam, Ab129267, 1:1000). We used an HRP (Horseradish peroxidase)–conjugated antibody (Bio-Rad 1:2000 in 1% milk-TBS-T) to detect the primary antibodies. For visualization we used an enhanced chemiluminescent substrate for detection of HRP (Pierce ECL Immuno-Blotting Substrate, Thermo Scientific). Expression levels of eNOS and Ercc1 were normalized to actin and cofilin. Lung protein of an Ercc1^{-/-} full body knockout mouse was used as a negative control for background subtraction.

For immunohistochemical stainings, aortic and kidney tissues were fixed in 4% buffered formaldehyde for 24 h, embedded in paraffin, and sectioned at 5 µm. After deparaffinization and rehydration, all sections were incubated in antigen retrieval buffer (pH 9) for 15 min at 100°C. Endogenous peroxidase was blocked by incubating the sections in 3% H₂O₂ in methanol for 10 min. For immunohistochemical staining the slides were blocked for 1 h and stained with P21 (1:100, ab107099) overnight at 4°C. Sections were incubated for 1 h at room temperature with the corresponding biotinylated secondary antibody (1:200, Vector BA-9400 and Dako E0432). After ABC (Vectastain PK-6100) incubation of 30 min, sections were subjected to DAB staining (Dako K3468). Images were acquired using Nanozoomer software and analyzed with NDP view 2.

ROS, H₂O₂, and superoxide measurement

Various markers of oxidative stress were assessed as previously described [29,30]. Briefly, superoxide anion (O₂⁻) production was measured in lung tissues (rich in ECs) by lucigenin chemiluminescence assay. This assay uses NADPH as the substrate and accordingly the chemiluminescence signal reflects NADPH-dependent O₂⁻ generation and is a measure of NADPH oxidase (Nox) activity. Nox is a major source of ROS in vascular cells. Hydrogen peroxide (H₂O₂) levels were measured by Amplex Red assay. Global O₂⁻ levels in cell homogenate were measured by electron paramagnetic resonance (EPR) in samples containing 10 µg of protein and 1 mM CMH (Enzo Life Sciences, U.K.) in a total volume of 100 µl of Krebs–HEPES buffer containing 25 µM deferoximine and 5 µM diethyldithiocarbamate (DETC). After homogenization, EPR samples were placed in 50 µl glass capillaries and measurements were performed by Bruker BioSpin's e-scan EPR (Bruker[®] Biospin Corp.) equipped with a super-high Q microwave cavity at room temperature. The EPR instrument settings for experiments were as follows: field sweep, 50 G; microwave frequency, 9.78 GHz; microwave power, 20 mW; modulation amplitude, 2 G; conversion time, 656 ms; time constant, 656 ms; 512 points resolution and receiver gain, 1 × 10⁵. Results were normalized by protein content.

Statistical methods

Data are presented as mean and standard error of the mean, unless otherwise indicated. Statistical analysis between the groups of single values was performed by unpaired, two-tailed *t* test. Differences in dose–response curves were tested by general linear model for repeated measures (sphericity assumed). Differences were considered significant at *P* < 0.05.

Results

General health features

There were no general signs of developmental problems in EC-KO, and body weight was normal until 5 months of age (Figure 1A). Blood cell analyses revealed no significant changes (Supplementary Table S2). However, EC-KO had a strongly reduced lifespan, with a median of 24.6 weeks (Supplementary Figure S1). Shortly before death, immobility and rapid breathing was observed in two of the EC-KO mice. Most deaths occurred at night. One of the two moribund mice, aged 22.6 weeks, was timely killed to undergo full body pathological examination. Organs included were brain, heart, skeletal muscle, aorta, sciatic nerve, liver, spleen, lung, and kidney. Again, no signs of developmental problems

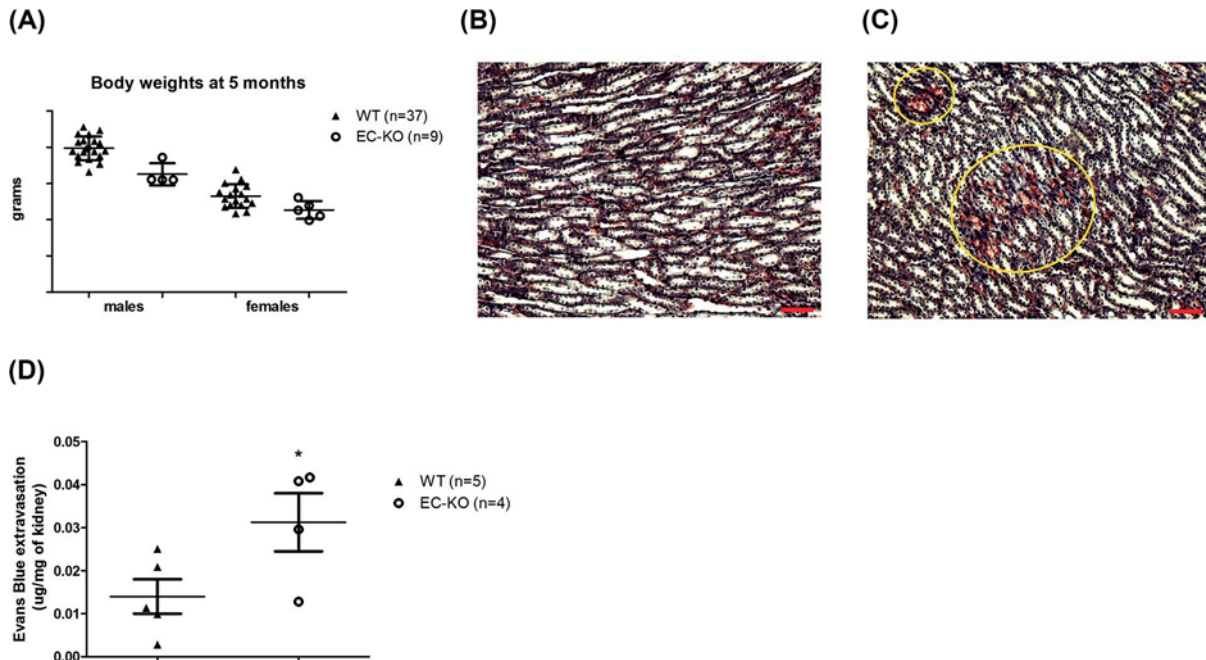


Figure 1. General health and pathology findings

Body weights at 5 months ($n=9$ EC-KO, 4 males and 5 females, and 37 WT, 19 males and 18 females) (A). Masson's trichrome staining of kidney sections from a control mouse (B) and an EC-KO mouse. (C) The area encircled shows extravasation of red blood cells in the proximity of the tubules. Kidney sections from five EC-KO and six WT mice were examined. (D) Renal Evans Blue leakage (μg Evans Blue \times mg of kidney tissue) 24 h after intravenous injection, results are expressed as means \pm SE. * P -value ≤ 0.05 compared with WT group.

were observed. Except for necrosis observed in the medulla of the kidney, the examined organs did not show morphological or histological aberrations. In three out of five EC-KO vs. one out of six WT of 5 months of age the kidney revealed red blood cells in the tubules (Figure 1B,C), indicating microvascular leakage in EC-KO. These data suggest that endothelial DNA repair deficiency impairs the permeability of the renal medullary microvasculature.

Renal vascular permeability

To corroborate the increased permeability of the renal vasculature we used an *in vivo* Evans Blue tissue penetration assay, comparing the vessel leakage between EC-KO and WT mice (5-month-old mice) in kidneys. The difference in vessel permeability was quantified spectrophotometrically by measuring the Evans Blue that was captured per gram of tissue. Our results show an increase in dye leakage from the kidney vessels of EC-KO mice when compared with WT mice (Figure 1D, P -value = 0.05).

In vivo microvascular function

To further examine peripheral microvascular function we performed laser Doppler reactive hyperemia studies. At 3 months of age there was no difference in reactive hyperemia in the hindlimb skin between EC-KO and WT (Figure 2A,B,E,F). At 5 months EC-KO showed decreased reactive hyperemia (Figure 2C–F). When passing from the age of 3–5 months reactive hyperemia tended to increase in WT mice, whereas it tended to decrease in EC-KO mice. In addition, lung perfusion was measured in WT ($n=4$) and EC-KO mice ($n=7$) showing significantly decreased lung perfusion in EC-KO mice (Figure 3A–C). The evaluation of reactive hyperemia in the WT group showed no differences between $\text{Cre}^+ \text{Ercc1}^{f/+}$ and the other control genotypes.

Ex vivo vasodilator responses in aorta and iliac arteries

To examine vasodilation in large arteries and reveal the mechanism of vasodilator dysfunction *ex vivo* organ bath experiments were performed. Aorta and iliac artery of EC-KO showed decreased endothelium-dependent relaxations to ACh compared with WT at the age of 5 months, which were still absent at 3 months of age (Figure 4A,B). Vas-

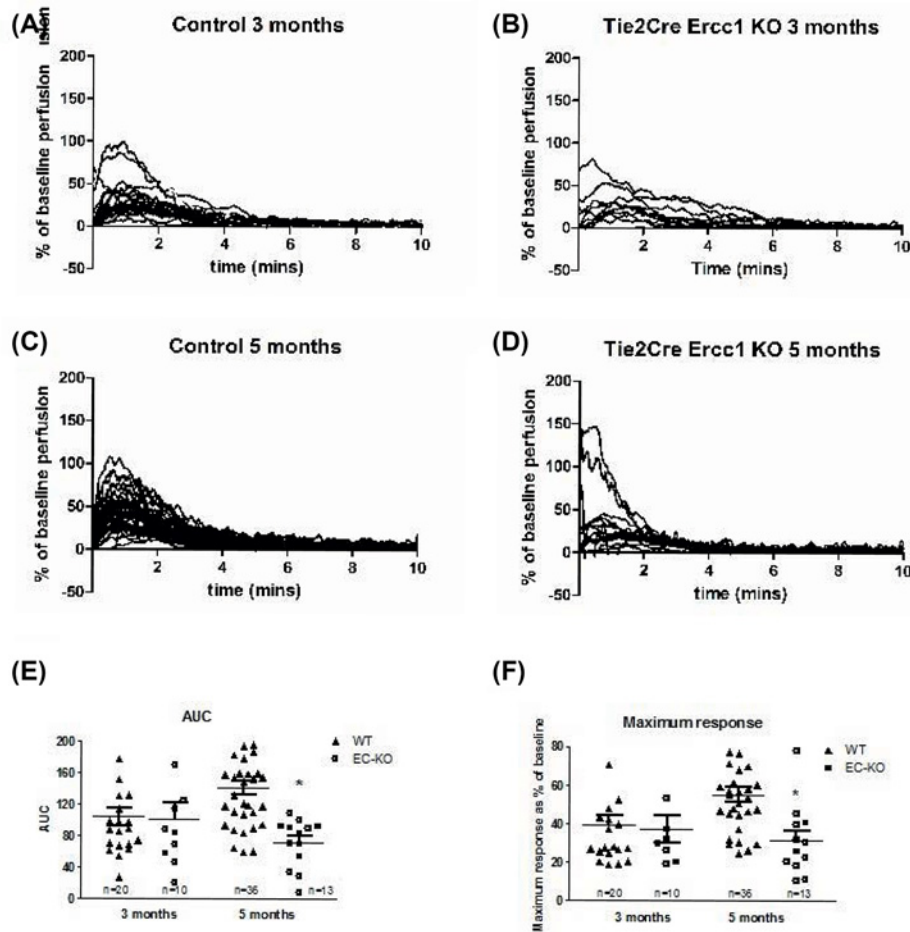


Figure 2. *In vivo* vasodilator function was assessed using Laser Doppler perfusion imaging

Functional differences between skin reperfusion after 2-min occlusion between WT (A) and EC-KO (B) at 3 months, and between WT (C) and EC-KO (D) at 5 months. Calculated area under the curve (E) and average maximum response (F) for the observed differences in skin reperfusion. * $P < 0.05$ (t test EC-KO vs WT). At 3 months, 10 EC-KO and 20 WT mice were examined. At 5 months, 13 EC-KO and 36 WT mice were examined.

cular smooth muscle dilatory function to the NO donor SNP was intact at both ages (Figure 4C,D). In WT mice, approximately half of the ACh response was mediated by NO (response to ACh was reduced by ~50% in the presence of the eNOS inhibitor L-NAME) (Figure 5A). No apparent contribution of prostaglandins was observed since the COX inhibitor indomethacin did not further reduce vasodilator responses (Figure 5A). Compared with WT mice, in EC-KO there was no contribution of the NO or prostaglandin pathways to the ACh responses (Figure 5B). In both WT and EC-KO, a residual ACh response was observed that was similar in both groups of mice, suggesting that the contribution of endothelium-derived hyperpolarizing factors (EDHFs) is intact.

We found no differences in the *ex vivo* vasodilatory responses between $Cre^+ Ercc1^{fl/+}$ and the rest of genotypes in the WT group (not shown).

The reduced NO availability and vasodilator dysfunction EC-KO mice could be explained by oxidative stress. NAC resulted in a leftward shift (pEC_{50} control -6.996 ± 0.1215 ($n=9$) vs. NAC -7.825 ± 0.2451 ($n=10$), $P < 0.05$) of the ACh dose response in EC-KO mice (Figure 5C), but not in WT littermates. These findings suggest a role for ROS in impaired vasodilation in EC-KO. PEG-CAT had no effect on ACh responses in EC-KO (Figure 5D) indicating that H_2O_2 is likely not important in altered vasodilation in these mice.

To further examine the role of oxidative stress we measured NADPH-dependent ROS generation by lucigenin chemiluminescence, O_2^- levels by EPR and H_2O_2 by Amplex Red. This was done in lung tissue, which is relatively rich in ECs, and which clearly shows reduced perfusion (Figure 3A–C). O_2^- and H_2O_2 levels were not different

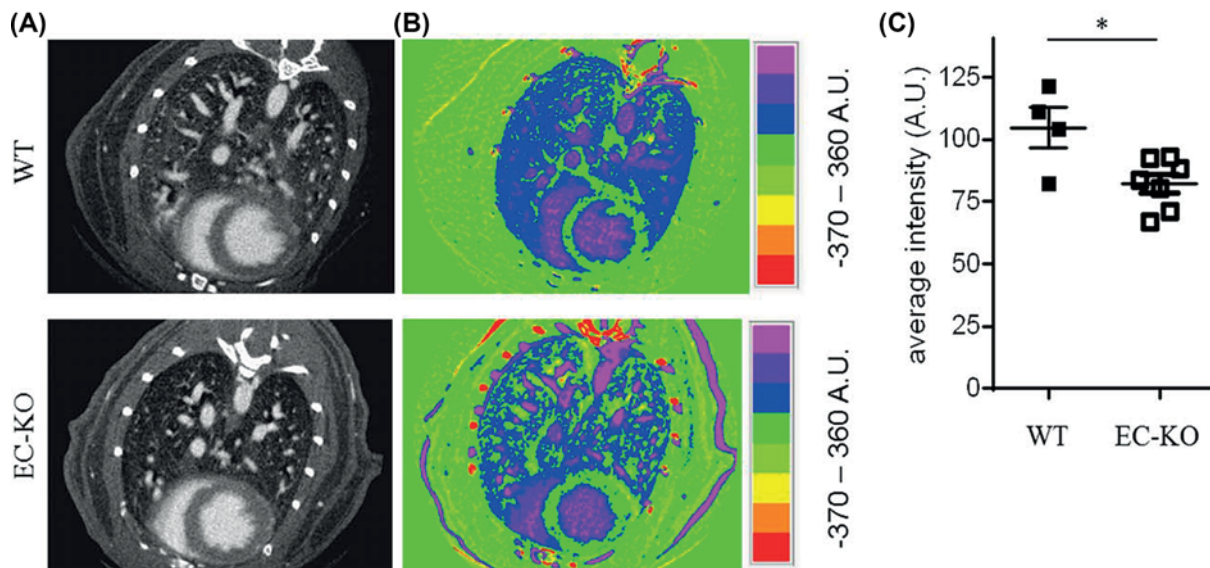


Figure 3. μ CT-based contrast-aided perfusion

μ CT-based contrast images of WT and EC-KO lungs (A). μ CT-based contrast-aided perfusion images of WT and EC-KO lungs, showing average intensity of perfusion after subtraction of the contrast to non-contrast images as the color bar indicates (B). Scatter plots depicting average intensity as a measure for lung perfusion, which is significantly reduced in EC-KO compared with WT. * $P < 0.05$ (t test EC-KO vs WT) (C). Seven EC-KO and four WT mice were included for these measurements.

between EC-KO and WT (Supplementary Figure S2). However, NADPH-mediated O_2^- production, an index of Nox activity, was significantly elevated in EC-KO compared with WT mice (Figure 5E).

Ex vivo vasodilator responses in coronary arteries

As a representative for mid-sized arteries important for direct blood supply in vital organs relevant for CVD we examined coronary artery function. In coronary arteries endothelium-dependent relaxation to ACh was significantly decreased in EC-KO both at 3 and 5 months of age (Figure 6A, P -value = 0.009 and 0.0007, respectively). Endothelium-independent relaxations to SNP were unchanged (Figure 6B). To study other endothelium-dependent agonists than ACh and the mechanism of vasodilator dysfunction ADP β S (NO and EDH-dependent) and UTP γ S (EDH-dependent) were employed.

ADP β S relaxation curves were shifted rightward in EC-KO (Figure 6C, P -value = 0.03) but responses to UTP γ S remain unchanged (Figure 6D). Responses to ADP β S and UTP γ S in arteries precontracted with 30 mmol/l KCl were examined as to exclude EDH [24–26]. Maximal dilations to ADP β S were decreased in EC-KO vs. WT (Figure 6E), whereas dilations to UTP γ S were cancelled in both mouse strains (Figure 6F). This result confirms that UTP γ S is entirely dependent on EDH, and that NO-mediated responses are decreased in EC-KO.

Levels of eNOS, luminal endothelial coverage, and *Ercc1* expression

Immunoblot analysis showed a tendency toward reduced baseline pulmonary eNOS protein level in EC-KO vs. WT, but this did not reach statistical significance (Figure 7A). Also, the ratio of eNOS-activating phosphorylation of the serine residue at position 1177 (pSer¹¹⁷⁷-eNOS) to total eNOS protein was not different at baseline (Figure 7A). The luminal surface of the abdominal aorta from 5-month-old animals was investigated for endothelial denudation (5 WT vs. 5 EC-KO). Scanning EM of the luminal surface also did not reveal a loss of ECs (Figure 7B). ERCC1 protein expression of the conditional *Ercc1* KO allele was tested in homogenized lung tissue as a surrogate for endothelial knockout. ERCC1 protein was significantly lowered in 5-month-old EC-KO ($n=4$) compared with WT ($n=4$) (Figure 7C,D).

Ex vivo vasoconstrictor responses

We tested contraction responses in iliac arteries to ET-1, Ang II, and phenylephrine (Supplementary Figure S3). Although at the age of 5 months phenylephrine responses were significantly lower in EC-KO, implying an effect of

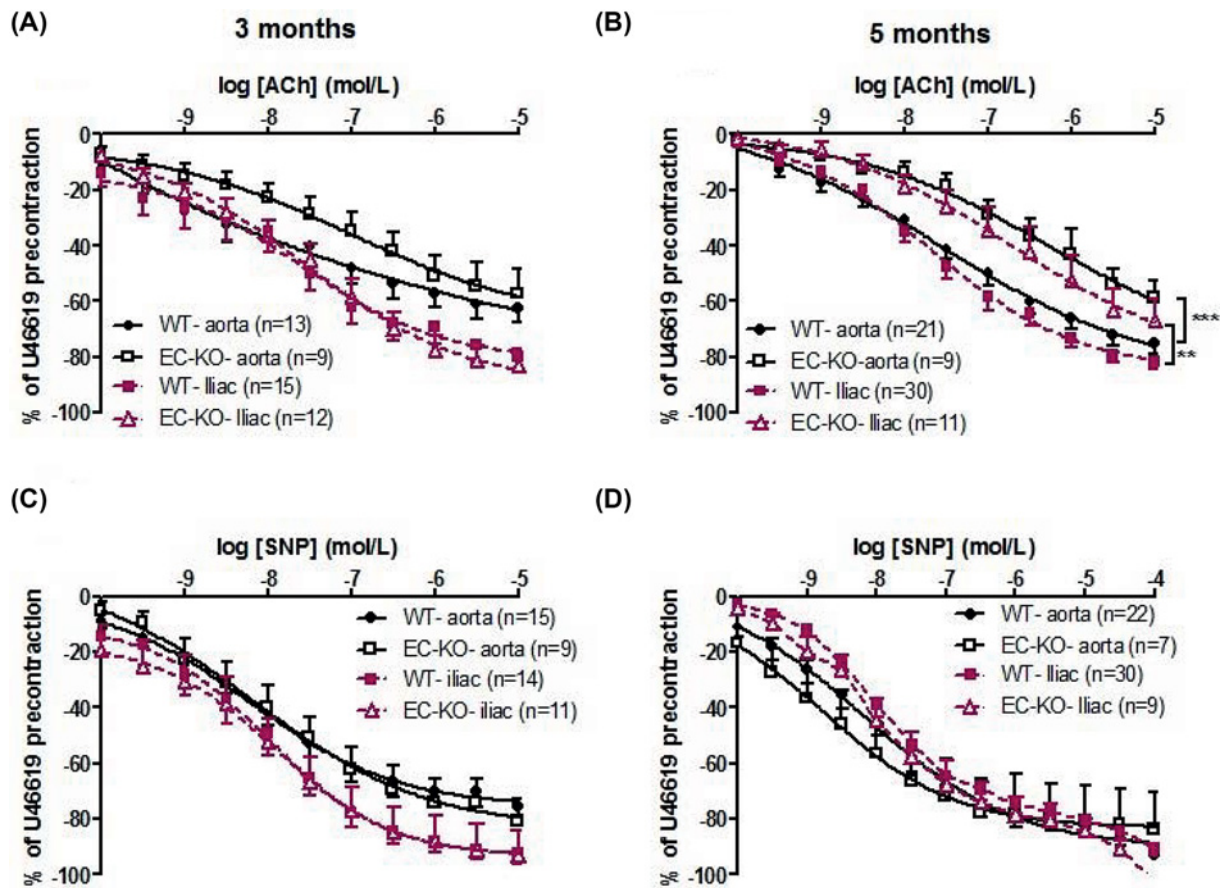


Figure 4. Endothelium-dependent and independent relaxations in isolated aortic and iliac rings measured *ex vivo* in organ bath set-ups

ACh-induced vasodilation of EC-KO and WT in aorta and iliac artery at 3 months (A) and at 5 months (B). Endothelial-independent relaxations induced by SNP in aortic and iliac rings at 3 months (C) and at 5 months (D). ** $P < 0.001$; *** $P < 0.0001$ (general linear model for repeated measures, sphericity assumed; EC-KO- aorta vs WT-aorta and EC-KO- iliac vs WT-iliac). At 3 months arteries from 9 to 12 EC-KO and 12 to 15 WT were studied. At 5 months arteries from 7 to 11 EC-KO and 21 to 30 WT were studied.

endothelial dysfunction on VSMC, we saw no consistent differences between WT and EC-KO of 3 and 5 months of age.

Mechanical properties and dimensions of the vascular wall

Since we previously found that arterial stiffness was increased in *Ercc1*^{Δ/-} mice [11], we measured aortic wall movement during cardiothoracic echography, and calculated distensibility of the aorta. At 3 months no differences were found between EC-KO and WT but at 5 months distensibility was decreased in EC-KO despite normal pulse pressures (Table 1). Since echography was not accompanied by simultaneous BP measurements, which are needed for indexation of aortic distensibility, we further evaluated the mechanical properties of aortic rings in organ baths. We confirmed that aorta of EC-KO was stiffer than that of WT (Figure 5F). Instead carotid arteries did not show significant differences in stiffness, lumen diameter or wall thickness under similar perfusion pressure increments between EC-KO and WT. Likewise, no differences in media strain or stress were observed (Supplementary Figure S4).

To determine if the higher stiffness of aorta was associated with structural remodeling, the dimensions of transversally sectioned aortic segments were measured. This was done in sections taken from the part adjacent to the segment used for stiffness measurement. Wall thickness was not significantly increased (Figure 8A). Vascular diameter showed

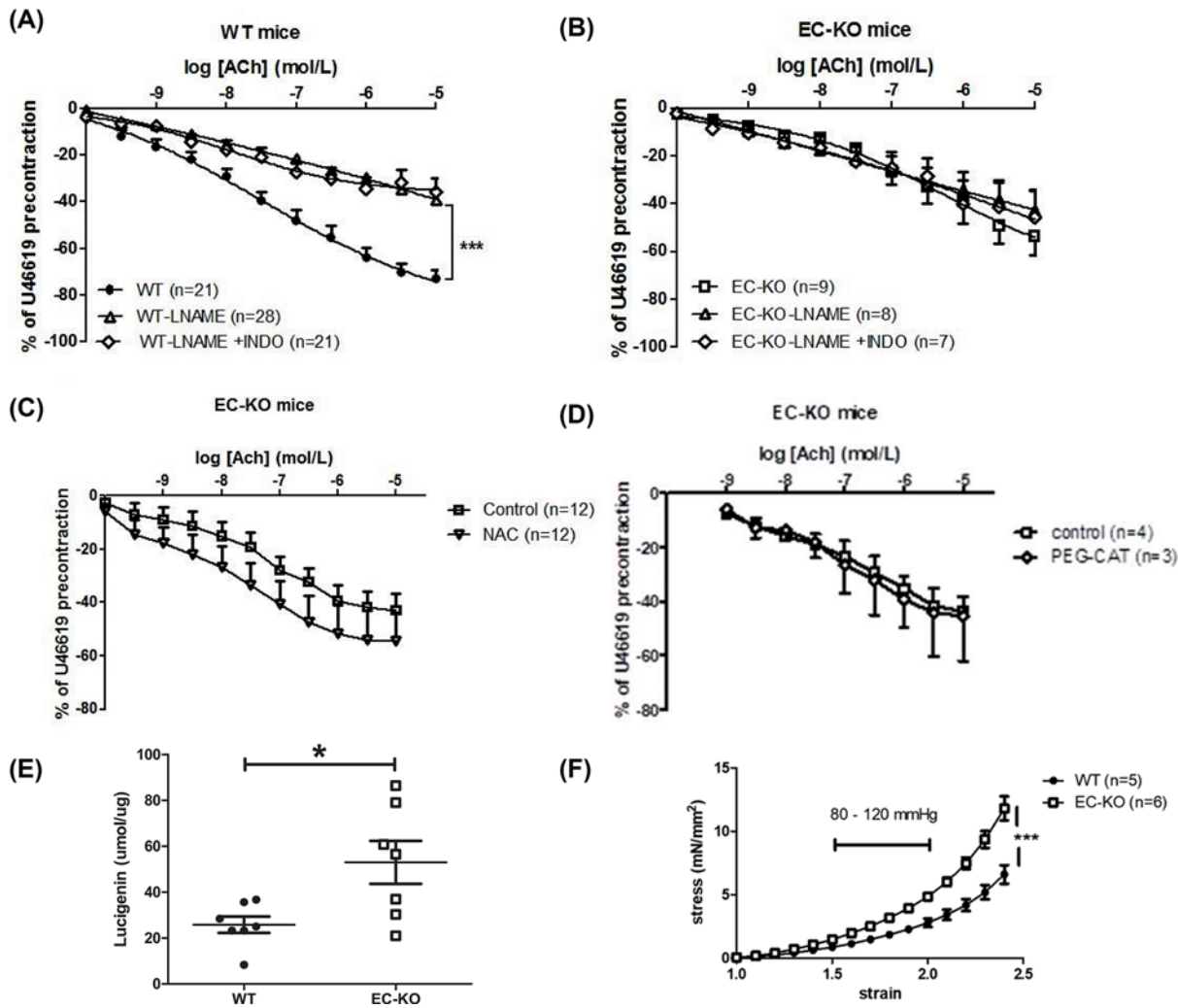


Figure 5. Contribution of NO, prostaglandins and oxidative stress to the endothelium-dependent vasodilations
 At 5 months, we evaluated the contribution of NO and prostaglandins to ACh-induced vasodilation in WT (A) and EC-KO (B). Vasodilator response in the presence of the wide range free radical scavengers (NAC) (C) and the H₂O₂ scavenger PEG-catalase in EC-KO mice (D). (E) Superoxide levels measured in lung tissue. * $P < 0.05$, t-test. (F) Aortic stress–strain relationship measured ex vivo in small wire organ bath set-up. The strain range corresponding to 80–120 mmHg pressure is indicated with the horizontal range bar. *** $P < 0.0001$ (general linear model for repeated measures, sphericity assumed; the responses to ACh alone were compared with the responses to ACh after preincubation with L-NAME). Aorta arteries from 7 to 12 EC-KO and 21 to 28 WT were studied.

a trend to be increased in EC-KO, being statistically significant for external diameter (Figure 8B,C). Transversal surface area was higher in EC-KO than in WT aorta (Figure 8D). Vessel circumference also increased, showing a significant increase in external circumference (Figure 8E,F). Hence, EC-KO showed a hypertrophic aorta wall featured by outward remodeling.

BP

Systolic BP (SBP) was higher in EC-KO at 3 months (138 mmHg in EC-KO vs 125 mmHg in WT mice) whereas no differences were observed at 5 months (P -value SBP = 0.72). No differences were observed in diastolic BP (DBP) at 3 or 5 months (Table 1).

Cardiac function

The change in SBP followed a biphasic course, being slightly elevated at 3 months and returned to normal at a time when endothelium-dependent vasodilation was markedly reduced (5 months). Therefore, we investigated cardiac

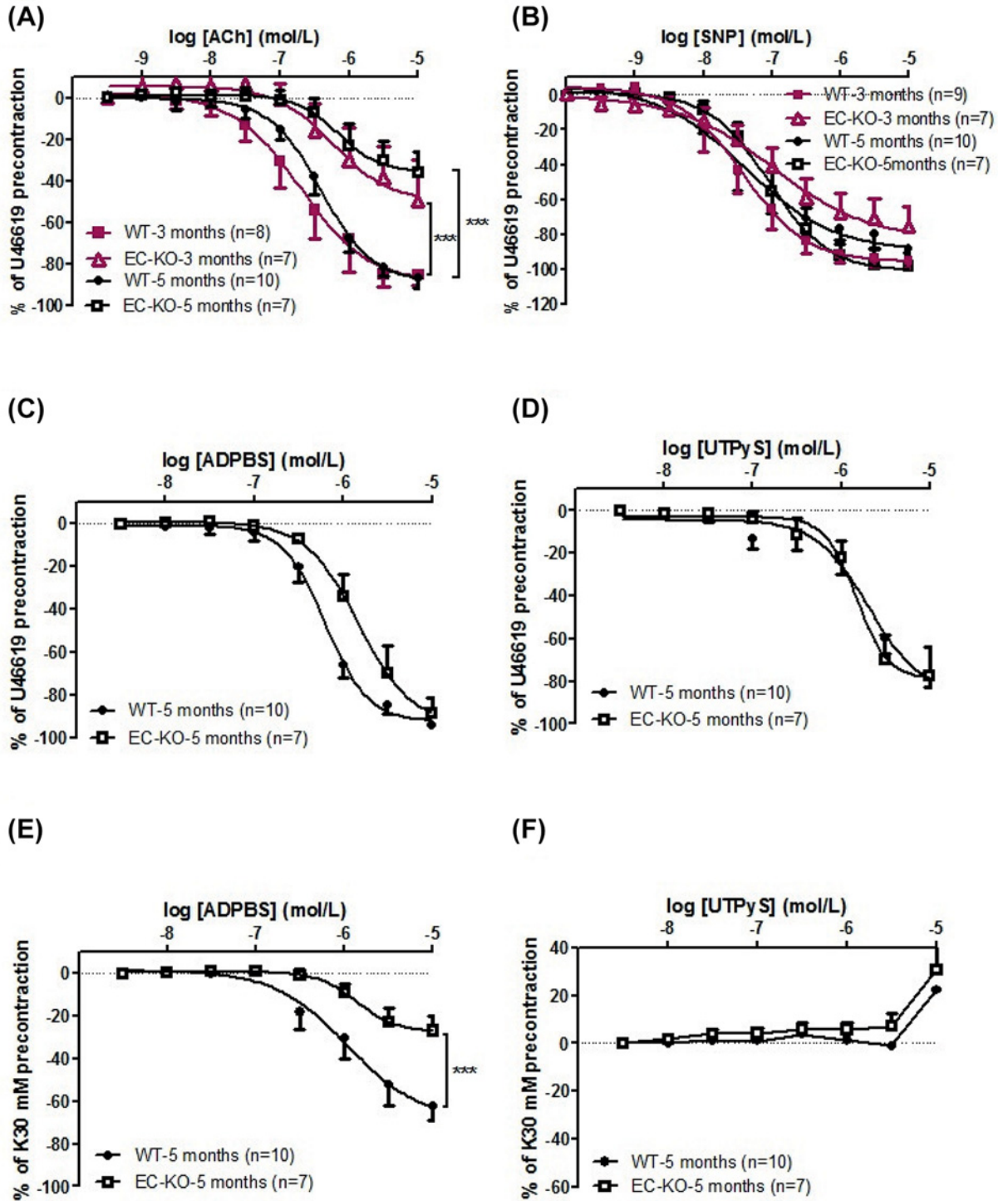


Figure 6. Vasodilation in coronary arteries measured ex vivo in small wire organ bath set-ups

Relaxations to ACh (A), SNP-induced vasodilatation (B), ADPβS (C) and UTPγS (D) in coronary rings precontracted with U46619. Relaxations to ADPβS (E) and UTPγS (F) in coronary rings precontracted with KCl 30 mM. *** $P < 0.0001$ (GLM-RM, EC-KO- 3 months vs WT- 3 months and EC-KO- 5 months vs WT- 5 months). At 3 months, coronary arteries from seven EC-KO and eight to nine WT were studied. At 5 months, arteries from seven EC-KO and ten WT were studied.

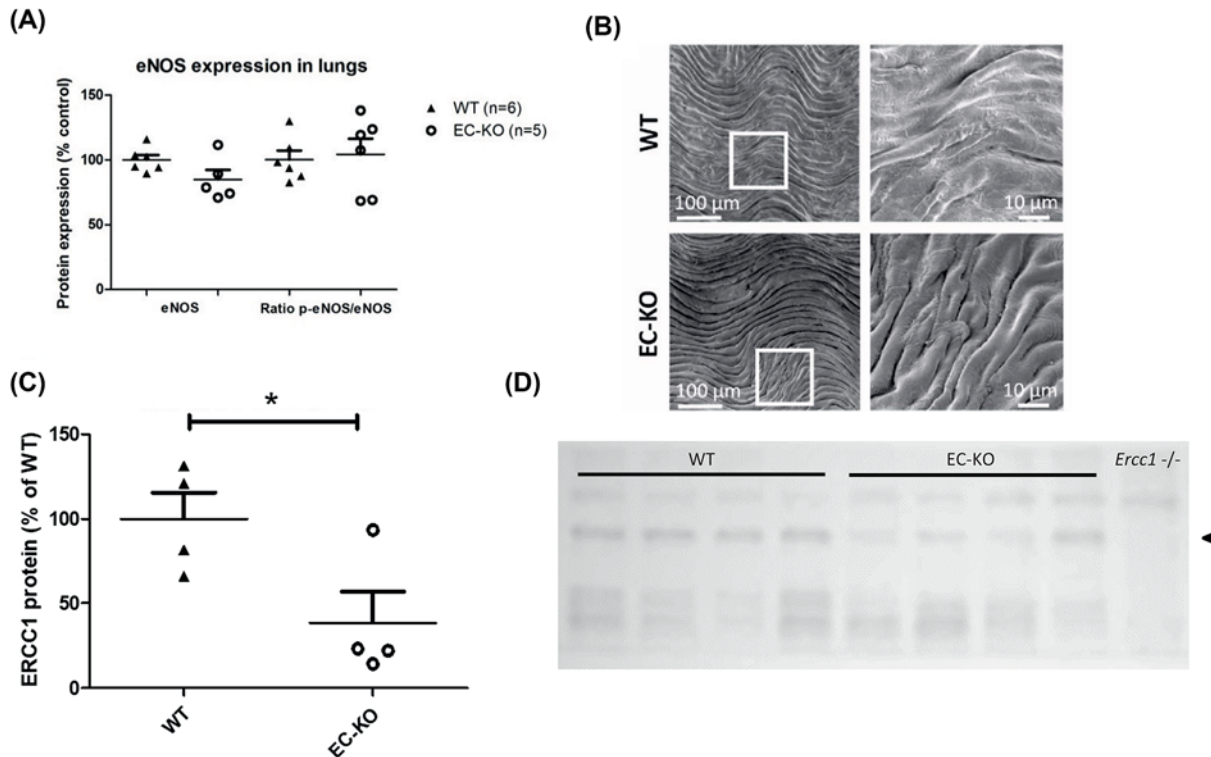


Figure 7. Levels of eNOS and scanning EM

Protein expression levels expressed as % of WT control in lung of (A) eNOS and p-eNOS over actin ($n=5$ EC-KO and 6 WT), (B) representative scanning EM images of the endothelium ($n=5$ EC-KO and 5 WT) and (C) expression of ERCC1 (arrowhead) ($n=4$ for both WT and EC-KO). * $P < 0.05$, t test. (D) Representative blot of ERCC1.

Table 1 Cardiac function, BP, and aorta distensibility at 3 and 5 months

Parameter	3 months			5 months		
	EC-KO ($n=10-19$)	WT ($n=11-21$)	P -value	EC-KO ($n=11-17$)	WT ($n=12-31$)	P -value
Stroke volume (μ l)	33 (5.5)	36 (5.1)	0.21 [‡]	32 (8.0)	36 (5.0)	0.01[‡]
Stroke volume index (μ l/mg myocardium)*	30 (4.5)	31 (4.1)	0.56 [§]	25 (5.2)	30 (3.5)	0.03[§]
Stroke volume index (μ l/g) [†]	1.4 (0.2)	1.4 (0.2)	0.81 [§]	1.2 (0.2)	1.3 (0.2)	0.49 [§]
Fractional shortening (%)	34 (5.1)	34 (5.7)	0.71 [§]	33 (6.5)	33 (6.0)	0.94 [§]
HR (bpm)	502 (37.4)	492 (37.0)	0.38 [§]	494 (40.1)	498 (49.2)	0.78 [§]
Cardiac output (ml/min)	17 (2.9)	18 (3.3)	0.24 [‡]	16 (4.1)	18 (3.6)	0.01[‡]
Cardiac index (ml/min/mg myocardium)*	15 (2.3)	15 (2.6)	0.92 [§]	13 (2.4)	14 (1.7)	0.06 [§]
Cardiac index (ml/min/g) [†]	0.7 (0.1)	0.7 (0.1)	0.93 [‡]	0.6 (0.1)	0.6 (0.1)	0.46 [§]
Heart weight (mg)	112 (12.8)	116 (17.1)	0.45 [§]	125 (25.3)	122 (20.2)	0.77 [§]
SBP (mmHg)	138 (14.6)	125 (11.9)	0.04 [§]	128 (22.8)	125 (20.6)	0.72 [§]
DBP (mmHg)	94 (15.2)	89 (15.6)	0.46 [§]	88 (19.3)	86 (20.7)	0.86 [§]
Aorta distensibility (mm)	0.3 (0.1)	0.3 (0.04)	0.69 [§]	0.2 (0.1)	0.3 (0.1)	0.05[§]

Values are mean (SD). Abbreviations: bpm, beats per minute; DBP, diastolic BP; HR, heart rate; SBP, systolic BP. Statistically significant outcomes are indicated in bold typesetting.

*Values are corrected for heart weight, expressed as per 100 mg of heart weight.

[†]Values are corrected for body weight, expressed as per gram of body weight.

[‡]Two-way ANNOVA.

[§] t test.

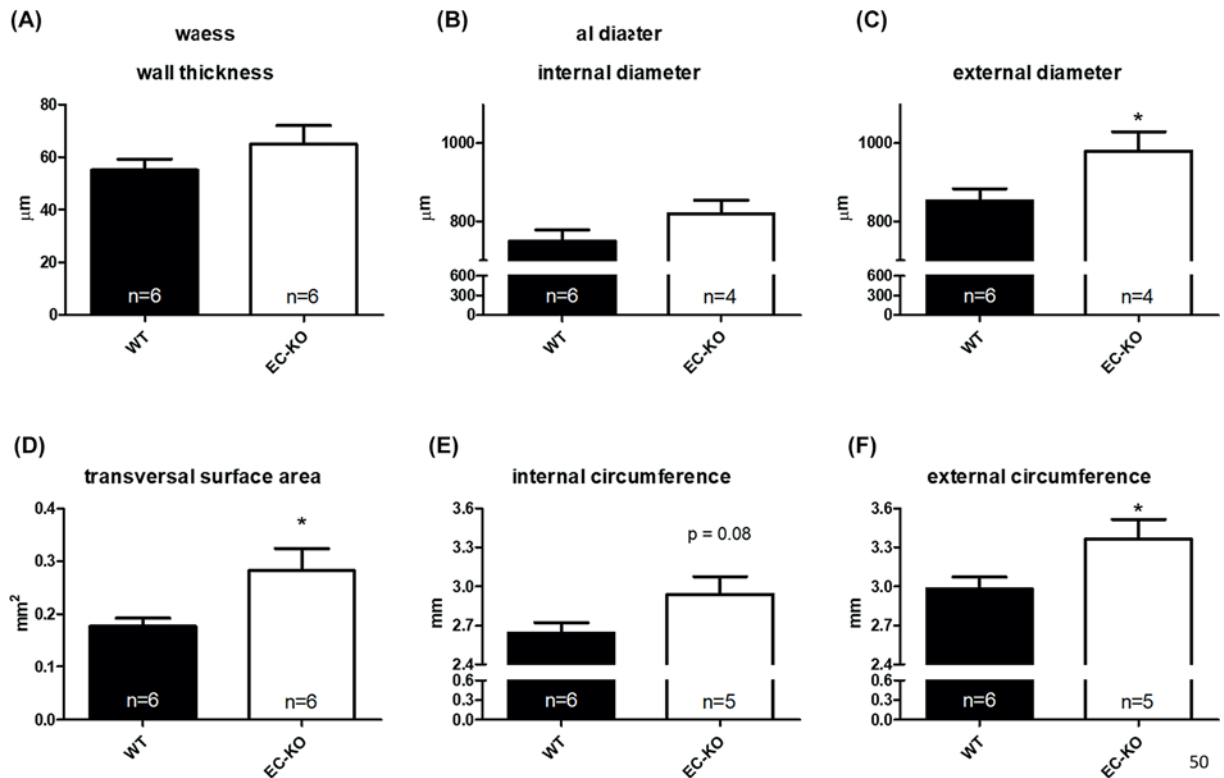


Figure 8. Aortic wall dimensions

All measurements were performed on Eosin-stained cryosections at 50× magnification using calibrated QWin software (Leica, Germany). (A–F) Depict the various dimension variables as indicated above the panels. ‘Internal’ and ‘External’ refer to the use of respectively the internal and external border of the *lamina media* as reference points for the measurements. *; $P < 0.05$, *t* test.

function, measuring volume variables, as a possible explanation. Since male and female mice have a different heart volume and weight, both two-way ANOVA including genotype and sex, were used as statistical corrections for these variables. No differences between EC-KO and WT were observed at 3 months. However, stroke volume (SV) and cardiac output (CO) were significantly decreased in 5 month-old EC-KO compared with WT (Table 1). In agreement, SV and CO indexed for heart weight were also decreased. When indexed for body weight however, SV and CO were equal between EC-KO and WT (Table 1). To exclude a sex-specific effect of *Ercc1* knockout we analyzed males and females separately, and found that that CO and SV were lowered in EC-KO for both sexes (data not shown). Indexed CO and SV were unchanged per sex. Given that FS and HW were normal we conclude that there was no cardiac dysfunction. However, since non-indexed and heart weight-indexed CO and SV were significantly or borderline significantly ($P=0.06$) lowered, we cannot rule out that cardiac function adapted to decrease the BP at 5 months of age.

Endothelial DNA damage response

To study if Tie2Cre-driven *Ercc1* removal leads to an endothelial DNA damage response we performed immunohistochemistry on the damage response marker p21, a marker that is associated with cellular senescence, in aorta. We stained four randomly taken sections of thoracic aorta per mouse, using five mice per genotype (EC-KO or WT littermate). Controls incubated with secondary antibody alone were negative (not shown). When incubated with both primary and secondary antibodies, we found that aortic sections in $n=4$ out of $n=5$ EC-KO contained scattered p21-positive ECs (Figure 9A), whereas all WT mice ($n=5$) were devoid of positive cells (Figure 9B). There were no positive cells outside the endothelium, demonstrating the specificity for vascular ECs. Since leakage studies with Evans Blue revealed that the renal vasculature was also affected, we stained four randomly taken renal tissue section for p21 for each of $n=5$ mice. In five out of five EC-KO mice positive cells were detected, scattered over glomeruli and in vascular lumen (Figure 9C,D), whereas WT ($n=5$) kidneys were all negative (Figure 9E). The localization

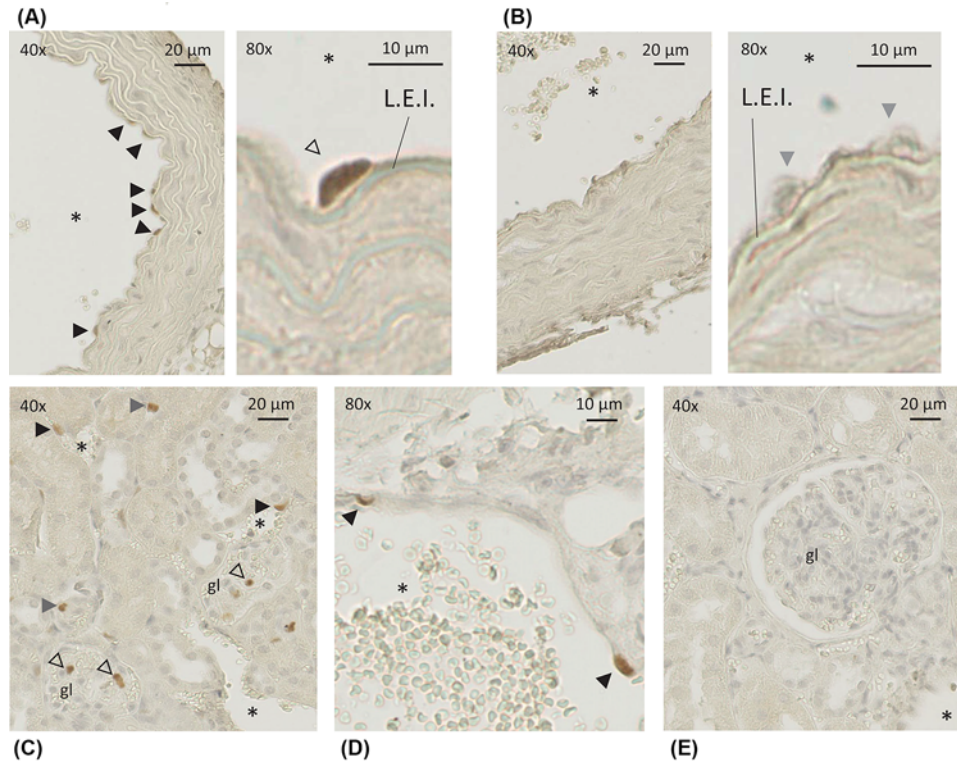


Figure 9. P21 staining

Photographs (A–C) show p21 staining in aortic tissue of EC-KO (A) and WT (B). The endothelial localization is evident at 40 \times magnification (closed arrowheads) and at larger magnification (80 \times) the nuclear localization of p21 is visible (A, open arrowhead). The p21-positive cell in (A) display the typical cobblestone appearance and localization on the *lamina elastica interna* (L.E.I.), identifying the positive cells as ECs. WT show p21-negative EC nuclei (B, gray arrowhead). Photographs (C–E) show p21 staining in the kidney in EC-KO (C,D) and WT (E). p21-positive cells are present along vascular lumen (closed arrowheads), along tubuli (gray arrowheads) and in glomeruli (gl; open arrowheads) (C). (D) shows positive cells along the lumen of the vessel wall at higher magnification. WT mice did not present positive cells (E). Asterisks mark vascular lumen.

of the positive cells along vascular lumen indicates that renal ECs were affected. Since glomeruli consist largely of endothelium, it seems likely that the p21-positive cells are ECs as well.

It is generally believed that dysfunction of ECs during aging contributes to a pro-inflammatory lamina media of the vessel wall, and thus to hypertrophic vascular remodeling. We questioned if this occurs spontaneously in the absence of an exogenous pro-inflammatory stimulus, i.e. only by selective aging of endothelium. We tested expression of interleukin (IL) 1 α (IL-1 α), IL-6, and tumor necrosis factor α (TNF α) mRNA. We chose these mediators because they are associated with the SASP, the secretory phenotype of senescent cells. We did not observe changes in aortic expression of IL-1 α , IL-6, and TNF α (Supplementary Figure S5).

Discussion

We investigated the role of endothelial-specific DNA repair defectiveness on cardiovascular function in a mouse model with specific loss of *Ercc1* in vascular ECs. We found that local endothelial genomic instability caused progressive macrovascular and microvascular vasodilator dysfunction at least in part due to specific loss of endothelium-derived NO. Smooth muscle responses to exogenously supplied NO were intact. Reduced eNOS expression does not seem to play a major role. The preserved EC layer, as confirmed by scanning EM as well as normal EDHF-mediated vasodilation, excludes the loss of NO through reduced EC numbers as a possible explanation. The most likely cause for the loss of vasodilation is reduced NO availability in EC-KO due to scavenging by ROS. The blunted endothelium-mediated NO responses are associated specifically with expression of the DNA damage response, cell stress and potential senescence marker p21. Thus, DNA damage results in a cell autonomous effect on NO signaling that might drive vascular aging. The change of endothelial function appears to affect VSMC as well,

as evidenced by altered vasoconstriction, increased aortic stiffness, and aortic hypertrophic remodeling, important features of vascular aging. This appears to be independent of a pro-inflammatory phenotype of medial cells, because in EC-KO aorta mRNA expression of inflammatory mediators IL-6 and TNF α , important in vascular inflammation, was not increased.

Notably, the rate of development of vasodilator dysfunction is location-specific at 3 months of age, this dysfunction is observed in coronary arteries, but not in iliac artery, aorta, or the skin microvasculature. This suggests a non-developmental origin of the vasomotor dysfunction. Apart from location-specific effects with respect to the origin of the artery that was studied, we also found location-specific effects within the arterial specimen itself. The presence of p21 only in ECs, and the absence of decreased VSMC responses to NO upon stimulation with SNP suggests that a cell-autonomous effect is observed in EC-KO with regard to endothelium-derived NO. Previously, in the whole body *Ercc1* knockout strain, *Ercc1*^{Δ/-} [11], lowering of eNOS was observed in lung tissue. In ECs eNOS might mediate cell-autonomous effects. However, in EC-KO we only observed a statistically non-significant trend toward lowering of eNOS. It is known that eNOS reacts to aging in diverse ways, varying from increased expression to compensate for loss of vasodilator capacity due to NO scavenging by ROS in an early, compensated stage of endothelial aging, to decrease of eNOS and its activation in senescent cells [31–33]. The Cre-lox system does not remove the target gene with 100% efficiency, and indeed not all ECs in EC-KO are p21-positive. Moreover, not all p21-positive cells might be senescent; the presence of several markers in combination is needed to confirm senescence. Therefore, it might be that there were senescent cells with lower eNOS, but not enough to statistically demonstrate eNOS lowering. Hence, the possibility that the observed lowering of ACh responses is the result of both NO quenching in the context of oxidative stress and eNOS lowering cannot be excluded.

Apart from vasodilator dysfunction EC-KO showed a severely compromised microvascular barrier function in the kidney. This was confirmed by histological examination and Evans Blue permeability tests, established methods for this purpose [34]. Therefore, the aging-mimicking effect of endothelial *Ercc1* deletion is not restricted to loss of vasodilator function, but at least affects barrier function in the kidney as well. Through this mechanism, the DNA damage response might contribute to progressive kidney damage, in addition to decreased NO signaling, an important determinant of renal deterioration [35]. Interestingly, cell cycle arrest in tubular cells induced by p21 plays a role in acute kidney injury (AKI), and plasma p21 levels have been proposed as a biomarker for AKI and renal aging [36,37]. It was suggested that this might take place independently from DNA damage because of the dissociation of DNA damage detection through ATM signaling [36,38]. However, this only excludes double strand break repair to be involved, although recently also transcription stress related R-loops were found to trigger ATM activation [39]. The question if DNA damage is involved therefore remains open. Our present finding prompts the question if endothelial aging, either caused by DNA damage or other mechanisms, might be implicated in p21-driven renal injury, and warrants further inspection of renal pathophysiology in endothelium-specific accelerated aging models.

In search of other features of vascular aging we tested vascular stiffness. At 5 months of age, aortic strain measured by echography was reduced in EC-KO, suggesting increased vascular stiffness. This was confirmed by *ex vivo* stress and strain measurements in aorta. The increased stiffness might be caused by the hypertrophic remodeling that we also observed in EC-KO. In contrast to aorta, carotid arteries did not show a change in vascular stiffness, again pointing to location-dependent difference. Increase in arterial stiffness with age, detected as increase in pulse wave velocity (PWV), is considered as a solid marker of vascular aging in humans [40]. PWV can be measured over different regions, such as from carotid to femoral, from brachial to carotid and from brachial to femoral artery. The different modes of PWV measurement show differential associations with age. Although this could involve technical aspects during measurements, it cannot be excluded that differential rates of aging occur in diverse blood vessels. This is well known for plaque development. Internal mammary arteries, for example, are relatively resistant to atherosclerotic burden, which has been attributed to endothelial features [41]. Coronary artery and aorta are generally known to be more vulnerable to plaque development. It is tempting to speculate that a differential susceptibility of the endothelium to DNA damage contributes to these differences.

Many of the features described in the EC-KO mice including vascular dysfunction, arterial remodeling, aortic stiffness, and aging are typically associated with oxidative stress and increased activation of Noxs as demonstrated in various models of CVD [42]. Our findings here of increased NADPH-mediated O₂⁻ production support this notion and suggest that EC Nox activity may be increased in EC-KO mice. Putative mechanisms whereby ERCC1 deficiency influences Noxs remain unclear and warrant further investigation. Reasons why there were no changes in global levels of O₂⁻ and H₂O₂ in EC-KO mice are unclear but may reflect efficient global antioxidant capacity.

As highlighted previously, vascular aging and DNA damage response are closely associated, as indicated by various research strategies from animal experiments to human (genetic) epidemiological studies and observations in progeroid syndromes [4,11,43]. In Mendelian randomization studies, it was found that telomere length, an important

marker of genomic instability, plays a causal role in CVD [44]. Epidemiologic research in large populations linking DNA damage response markers specifically obtained from circulating ECs to various degrees of vascular dysfunction, eg. of vascular stiffness as measured by PWV, might provide important further evidence of the role of DNA damage in vascular aging. Epidemiological studies might also represent a future translational step of our findings as it could lead to development of markers that represent vascular age, which are potential tools for CVD risk prediction. Important in light of using ECs for such marker studies is our observation that the effect of DNA damage on NO signaling is specifically evoked within the endothelium, possibly even cell autonomously. Endothelium-specific markers might be an important addition to biomarker testing, such as inflammatory markers and telomere length, in white blood cells or in plasma, currently done in epidemiological studies that address vascular age and CVD risk [44]. Whether this concerns only endothelial DNA damage response markers or also inflammatory markers, is an important question. A limitation of our study is that we were unable to explore mRNA of inflammatory factors specifically in the endothelium (isolation of EC or their RNA was technically not feasible, data not shown). We cannot, however, exclude the possibility that due to cell-autonomous effects ECs may assume a pro-inflammatory phenotype. Increased vascular leakage is suggestive of this and warrants further exploration.

Despite cell autonomous effects on NO signaling, changes in EC-KO were not restricted to endothelial function alone, as witnessed by hypertrophic vascular remodeling in aorta, changes in constrictions, but also the renal changes. EC-KO share some features with *Ercc1*^{Δ/-} mice, including a worsened renal morphology and a shortened lifespan [9]. In an earlier publication rescuing the liver of *Ercc1* null mutant mice from genetic *Ercc1* inactivation, it was shown that next to the liver the renal tissue is exceptionally vulnerable to loss of *Ercc1* function, and it was suggested that renal problems might be an important cause of death in the ‘rescued’ mice [45]. Our present results indicate that endothelial DNA damage might contribute to the renal problems.

Another important feature of aging is increased BP. This appeared in EC-KO at 3 months of age, but was absent at 5 months. We observed clues that at 5 months SV and CO were adapted in EC-KO, possibly to normalize BP in a phase state during which widespread overt vasodilator dysfunction can be found. This might not have happened at 3 months of age since vasodilator function is not as widespread at that age. In earlier studies we observed a small increase in BP in *Ercc1*^{Δ/-} mice. Apparently, the loss of endothelium-derived NO can be corrected, e.g., by autonomic regulation.

In conclusion, we found that local endothelial genomic instability in mice reproduces important features of vascular aging that are also observed in humans. Increased vascular stiffness, vascular hypertrophic remodeling, loss of endothelium-dependent vasodilation, increased vascular leakage, and the differential vulnerability of various arteries are among the most important characteristics. Our present study adds to the growing evidence that the DNA damage response plays a central role in vascular aging, and that aging pathology can be driven by genome instability and persistent DNA damage in a cell-autonomous manner in a variety of organs and tissues [46–50]. We propose epidemiological studies employing DNA damage response markers to further address the relevance in humans and provide a translational step towards CVD prediction markers. The loss of endothelium-derived NO and increased O₂⁻ bioavailability might play a major role in the observed phenotype. Further, we have shown that diet restriction is another potential treatment option, as this rescues loss of vasodilator function in *Ercc1*^{Δ/-} mice as well as in humans [8,12,51]. Therefore, studies exploring the impact of dietary restriction on DNA damage-induced vascular aging and the involved rescue mechanisms can be of great value.

Clinical perspectives

- We wanted to know if endothelial DNA damage causes features of vascular aging.
- We showed that endothelial DNA damage decreases endothelial-dependent vasodilations and end organ perfusion (lung and skin), increased vascular stiffness, vascular leakage (kidney), and wall thickness. The NO signaling pathway is specifically decreased. Superoxide formation, probably arising from Nox, and possibly also cellular senescence might play a role in the observed aging features.
- The observation that the vascular changes are associated with p21 increase is clinically relevant considering the development of senolytic drugs. The decreased NO, and increased superoxides, is important for the clinical development of drugs acting on these pathways, e.g. sGC activators and stimulators, PDE inhibitors, and Nox inhibitors. Similar to human aging, arteries are differentially affected in mice lacking endothelial DNA repair. The coronary artery is the most rapidly affected

vascular bed in our study and may have implications for coronary disease. Renal vascular leakage and necrosis were observed, which might have implications for aging-related renal dysfunction. Our findings further support the use of p21 as a clinical biomarker for kidney injury. Microvascular function is disturbed by the endothelial DNA repair defect and may have impact on aging-associated end organ dysfunction.

- Future clinical studies on DNA damage and repair in the human vascular system are warranted. In particular, epidemiologic biomarker research specifically in ECs might provide further evidence of the role of DNA damage and repair in CVD, and might be of additional value when optimizing CVD risk prediction.

Competing Interests

The authors declare that there are no competing interests associated with the manuscript.

Funding

This work was supported by the Netherlands CardioVascular Research Initiative: an initiative with support of the Dutch Heart Foundation [grant numbers CVON2011-11 (ARENA), CVON2014-11 (RECONNECT)]; the Colciencias Colombia, a grant under Call 617 of 2013 (to P.K.B.-N.); the Dutch Heart Foundation [grant number 2015T094 (to A.J.M.R. and J.J.v.d.L.)]; the TKI-LSH [grant number EMCLSH19013 (to A.J.M.R. and J.J.v.d.L.)]; the Stichting Lijf en Leven (to A.J.M.R. and J.J.v.d.L.); the Human Disease Model Award from Erasmus MC (to A.J.M.R. and J.J.v.d.L.); the British Heart Foundation Chair Award [grant number CH/12/4/29762 (to R.M.T.)]; the International Headache Society (to K.A.H.); the Czech Centre for Phenogenomics [grant number LM2015040 (to R.S.)]; Youth and Sports (MEYS) (to R.S.); the Academy of Sciences of the Czech Republic [grant number RVO 68378050]; the British Heart Foundation Fellowship (BHF) [grant number FS/15/60/31510 (to R.I.M.)]; the National Institute of Health (NIH)/National Institute of Ageing (NIA) [grant number PO1 AG017242 (to J.H.J.H.)]; and the European Research Council Advanced Grants DamAge and Dam2Age and Proof of Concept Grant Dementia, SFB628, Memorabel (ZonMW), BBoL (NWO-ENW), and ONCODE Supported by the Dutch Cancer Society.

Author Contribution

The contributions of the authors are as follows: A.J.M.R., A.H.J.D., I.v.d.P., R.M.T., A.C.M., D.J.D., K.A.H. and J.H.J.H. conceived the design of the study. P.K.B.-N. and E.P.-F. conducted and analyzed the *ex vivo* vascular experiments from aortas and iliacs arteries as well as immunoblots. P.K.B.-N. performed BP measurement and quantitative real-time PCR. J.J.v.d.L. performed p21 staining and histological examination thereof, performed western blots for ERCC1, designed these experiments, and wrote the methods and results part covering these data. E.P.-F. and R.I.M. assessed the blood vessel permeability. E.R.-B. and K.A.H. conducted and analyzed the *ex vivo* vascular experiments from coronary arteries. R.B. and R.d.V. were in charge of mice breeding and monitoring and evaluated the mechanical properties of the carotid vascular wall. R.v.V. performed cardiac function and BP measurements. R.d.V. and M.d.B. performed cardiac echography. M.D. performed detection of senescence markers. A.d.B., R.T. and R.I.M. performed renal and further tissue histological analyses. Y.R., I.v.d.P. and J.E. assessed the microvascular vasodilator function and lung perfusion *in vivo*. H.M.M.v.B. performed EM. R.M.T. and A.C.M. performed studies on ROS. M.G. and R.S. gave scientific advice and contributed to the writing of the manuscript.

Acknowledgements

We thank Mrs. Jacqueline Thomson of Glasgow of the University of Glasgow for her technical assistance. This work was supported through the use of imaging equipment provided by the Applied Molecular Imaging Erasmus MC facility.

Abbreviations

ADP β S, adenosine 5'-O-(2-thiodiphosphate); ACh, acetylcholine; Ang II, angiotensin II; BP, blood pressure; CVD, cardiovascular disease; CO, cardiac output; CRC, concentration–response curve; EC, endothelial cell; EC-KO, EC knockout; EDHF, endothelium-derived hyperpolarizing factor; EM, electron microscopy; eNOS, endothelial nitric oxide synthase; ERCC1, excision repair cross-complementation group 1; ET-1, endothelin-1; IL, interleukin; L-NAME, NG-nitro-L-arginine methyl ester; LV, left ventricular; NAC, N-acetyl-cysteine; NER, nucleotide excision repair; NO, nitric oxide; Nox, NADPH oxidase; PWV, pulse wave velocity; ROS, reactive oxygen species; SASP, senescence-associated secretory phenotype; SBP, systolic BP; SNP, sodium

nitroprusside; SV, stroke volume; TNF α , tumor necrosis factor α ; UTP γ S, uridine-5'-(γ -thio)-triphosphate; VSMC, vascular smooth muscle cell; WT, wild-type.

References

- 1 North, B.J. and Sinclair, D.A. (2012) The intersection between aging and cardiovascular disease. *Circ. Res.* **110**, 1097–1108, <https://doi.org/10.1161/CIRCRESAHA.111.246876>
- 2 Lopez-Otin, C., Blasco, M.A., Partridge, L., Serrano, M. and Kroemer, G. (2013) The hallmarks of aging. *Cell* **153**, 1194–1217, <https://doi.org/10.1016/j.cell.2013.05.039>
- 3 Hoeijmakers, J.H. (2009) DNA damage, aging, and cancer. *N. Engl. J. Med.* **361**, 1475–1485, <https://doi.org/10.1056/NEJMra0804615>
- 4 Bautista-Nino, P.K., Portilla-Fernandez, E., Vaughan, D.E., Danser, A.H. and Roks, A.J. (2016) DNA damage: a main determinant of vascular aging. *Int. J. Mol. Sci.* **17**, pii: E748, <https://doi.org/10.3390/ijms17050748>
- 5 Vermeij, W.P., Hoeijmakers, J.H. and Pothof, J. (2016) Genome integrity in aging: human syndromes, mouse models, and therapeutic options. *Annu. Rev. Pharmacol. Toxicol.* **56**, 427–445, <https://doi.org/10.1146/annurev-pharmtox-010814-124316>
- 6 Weeda, G., Donker, I., de Wit, J., Morreau, H., Janssens, R., Vissers, C.J. et al. (1997) Disruption of mouse ERCC1 results in a novel repair syndrome with growth failure, nuclear abnormalities and senescence. *Curr. Biol.* **7**, 427–439, [https://doi.org/10.1016/S0960-9822\(06\)00190-4](https://doi.org/10.1016/S0960-9822(06)00190-4)
- 7 Lans, H., Hoeijmakers, J.H.J., Vermeulen, W. and Marteijn, J.A. (2019) The DNA damage response to transcription stress. *Nat. Rev. Mol. Cell Biol.* **20**, 766–784, <https://doi.org/10.1038/s41580-019-0169-4>
- 8 Vermeij, W.P., Dollé, M.E., Reiling, E., Jaarsma, D., Payan-Gomez, C., Bombardieri, C.R. et al. (2016) Restricted diet delays accelerated ageing and genomic stress in DNA-repair-deficient mice. *Nature* **537**, 427–431, <https://doi.org/10.1038/nature19329>
- 9 Dollé, M.E.T., Kuiper, R.V., Roodbergen, M., Robinson, J., de Vlugt, S., Wijnhoven, S.W.P. et al. (2011) Broad segmental progeroid changes in short-lived *Erc1* Δ 7 mice. *Pathobiol. Aging Age Relat. Dis.* **1**, 7219
- 10 Niedernhofer, L.J., Garinis, G.A., Raams, A., Lalai, A.S., Robinson, A.R., Appeldoorn, E. et al. (2006) A new progeroid syndrome reveals that genotoxic stress suppresses the somatotroph axis. *Nature* **444**, 1038, <https://doi.org/10.1038/nature05456>
- 11 Durik, M., Kavousi, M., van der Pluijm, I., Isaacs, A., Cheng, C., Verdonk, K. et al. (2012) Nucleotide excision DNA repair is associated with age-related vascular dysfunction. *Circulation* **126**, 468–478, <https://doi.org/10.1161/CIRCULATIONAHA.112.104380>
- 12 Wu, H., van Thiel, B.S., Bautista-Nino, P.K., Reiling, E., Durik, M., Leijten, F.P.J. et al. (2017) Dietary restriction but not angiotensin II type 1 receptor blockade improves DNA damage-related vasodilator dysfunction in rapidly aging *Erc1* Δ mice. *Clin. Sci. (Lond.)* **131**, 1941–1953, <https://doi.org/10.1042/CS20170026>
- 13 Alva, J.A., Zovein, A.C., Monvoisin, A., Murphy, T., Salazar, A., Harvey, N.L. et al. (2006) VE-Cadherin-Cre-recombinase transgenic mouse: a tool for lineage analysis and gene deletion in endothelial cells. *Dev. Dyn.* **235**, 759–767, <https://doi.org/10.1002/dvdy.20643>
- 14 Tan, Z., Chen, K., Shao, Y., Gao, L., Wang, Y., Xu, J. et al. (2016) Lineage tracing reveals conversion of liver sinusoidal endothelial cells into hepatocytes. *Dev. Growth Differ.* **58**, 620–631
- 15 Taoudi, S., Gonneau, C., Moore, K., Sheridan, J.M., Blackburn, C.C., Taylor, E. et al. (2008) Extensive hematopoietic stem cell generation in the AGM region via maturation of VE-cadherin⁺CD45⁺ pre-definitive HSCs. *Cell Stem Cell* **3**, 99–108, <https://doi.org/10.1016/j.stem.2008.06.004>
- 16 Rybtsov, S., Sobiesiak, M., Taoudi, S., Souilhol, C., Senserrick, J., Liakhovitskaia, A. et al. (2011) Hierarchical organization and early hematopoietic specification of the developing HSC lineage in the AGM region. *J. Exp. Med.* **208**, 1305–1315, <https://doi.org/10.1084/jem.20102419>
- 17 De Palma, M., Venneri, M.A., Galli, R., Sergi, L.S., Politi, L.S., Sampaolesi, M. et al. (2005) Tie2 identifies a hematopoietic lineage of proangiogenic monocytes required for tumor vessel formation and a mesenchymal population of pericyte progenitors. *Cancer Cell* **8**, 211–226, <https://doi.org/10.1016/j.ccr.2005.08.002>
- 18 Zovein, A.C., Hofmann, J.J., Lynch, M., French, W.J., Turlo, K.A., Yang, Y. et al. (2008) Fate tracing reveals the endothelial origin of hematopoietic stem cells. *Cell Stem Cell* **3**, 625–636, <https://doi.org/10.1016/j.stem.2008.09.018>
- 19 Doig, J., Anderson, C., Lawrence, N.J., Selfridge, J., Brownstein, D.G. and Melton, D.W. (2006) Mice with skin-specific DNA repair gene (*Erc1*) inactivation are hypersensitive to ultraviolet irradiation-induced skin cancer and show more rapid actinic progression. *Oncogene* **25**, 6229–6238, <https://doi.org/10.1038/sj.onc.1209642>
- 20 Radu, M. and Chernoff, J. (2013) An *in vivo* assay to test blood vessel permeability. *J. Vis. Exp.* **73**, e50062, <https://doi.org/10.3791/50062>
- 21 Ezerina, D., Takano, Y., Hanaoka, K., Urano, Y. and Dick, T.P. (2018) N-acetyl cysteine functions as a fast-acting antioxidant by triggering intracellular H₂S and sulfane sulfur production. *Cell Chem Biol.* **25**, 447e444–459e444, <https://doi.org/10.1016/j.chembiol.2018.01.011>
- 22 Rieg, T., Gerasimova, M., Boyer, J.L., Insel, P.A. and Vallon, V. (2011) P2Y₂ receptor activation decreases blood pressure and increases renal Na⁽⁺⁾ excretion. *Am. J. Physiol. Regul. Integr. Comp. Physiol.* **301**, R510–R518, <https://doi.org/10.1152/ajpregu.00148.2011>
- 23 Faraci, F.M., Lynch, C. and Lamping, K.G. (2004) Responses of cerebral arterioles to ADP: eNOS-dependent and eNOS-independent mechanisms. *Am. J. Physiol. Heart Circ. Physiol.* **287**, H2871–H2876, <https://doi.org/10.1152/ajpheart.00392.2004>
- 24 Chen, G. and Suzuki, H. (1989) Some electrical properties of the endothelium-dependent hyperpolarization recorded from rat arterial smooth muscle cells. *J. Physiol.* **410**, 91–106, <https://doi.org/10.1113/jphysiol.1989.sp017522>
- 25 Corriu, C., Feletou, M., Canet, E. and Vanhoutte, P.M. (1996) Inhibitors of the cytochrome P450-mono-oxygenase and endothelium-dependent hyperpolarizations in the guinea-pig isolated carotid artery. *Br. J. Pharmacol.* **117**, 607–610, <https://doi.org/10.1111/j.1476-5381.1996.tb15233.x>
- 26 Kilpatrick, E.V. and Cocks, T.M. (1994) Evidence for differential roles of nitric oxide (NO) and hyperpolarization in endothelium-dependent relaxation of pig isolated coronary artery. *Br. J. Pharmacol.* **112**, 557–565, <https://doi.org/10.1111/j.1476-5381.1994.tb13110.x>
- 27 O'Rourke, M.F., Staessen, J.A., Vlachopoulos, C. and Duprez, D. (2002) Clinical applications of arterial stiffness; definitions and reference values. *Am. J. Hypertens.* **15**, 426–444, [https://doi.org/10.1016/S0895-7061\(01\)02319-6](https://doi.org/10.1016/S0895-7061(01)02319-6)

- 28 Fleenor, B.S., Sindler, A.L., Eng, J.S., Nair, D.P., Dodson, R.B. and Seals, D.R. (2012) Sodium nitrite de-stiffening of large elastic arteries with aging: role of normalization of advanced glycation end-products. *Exp. Gerontol.* **47**, 588–594, <https://doi.org/10.1016/j.exger.2012.05.004>
- 29 Neves, K.B., Rios, F.J., van der Mey, L., Alves-Lopes, R., Cameron, A.C., Volpe, M. et al. (2018) VEGFR (vascular endothelial growth factor receptor) inhibition induces cardiovascular damage via redox-sensitive processes. *Hypertension* **71**, 638–647, <https://doi.org/10.1161/HYPERTENSIONAHA.117.10490>
- 30 Griendling, K.K., Touyz, R.M., Zweier, J.L., Dikalov, S., Chilian, W., Chen, Y.R. et al. (2016) Measurement of reactive oxygen species, reactive nitrogen species, and redox-dependent signaling in the cardiovascular system: a scientific statement From the American Heart Association. *Circ. Res* **119**, e39–75, <https://doi.org/10.1161/RES.000000000000110>
- 31 Donato, A.J., Gano, L.B., Eskurza, I., Silver, A.E., Gates, P.E., Jablonski, K. et al. (2009) Vascular endothelial dysfunction with aging: endothelin-1 and endothelial nitric oxide synthase. *Am. J. Physiol. Heart Circ. Physiol.* **297**, H425–H432, <https://doi.org/10.1152/ajpheart.00689.2008>
- 32 Cernadas, M.R., Sanchez de Miguel, L., Garcia-Duran, M., Gonzalez-Fernandez, F., Millas, I., Monton, M. et al. (1998) Expression of constitutive and inducible nitric oxide synthases in the vascular wall of young and aging rats. *Circ. Res.* **83**, 279–286, <https://doi.org/10.1161/01.RES.83.3.279>
- 33 Minamino, T. and Komuro, I. (2007) Vascular cell senescence: contribution to atherosclerosis. *Circ. Res.* **100**, 15–26, <https://doi.org/10.1161/01.RES.0000256837.40544.4a>
- 34 Saria, A. and Lundberg, J.M. (1983) Evans blue fluorescence: quantitative and morphological evaluation of vascular permeability in animal tissues. *J. Neurosci. Methods* **8**, 41–49, [https://doi.org/10.1016/0165-0270\(83\)90050-X](https://doi.org/10.1016/0165-0270(83)90050-X)
- 35 Malyszko, J. (2010) Mechanism of endothelial dysfunction in chronic kidney disease. *Clin. Chim. Acta* **411**, 1412–1420, <https://doi.org/10.1016/j.cca.2010.06.019>
- 36 Yang, L., Besschetnova, T.Y., Brooks, C.R., Shah, J.V. and Bonventre, J.V. (2010) Epithelial cell cycle arrest in G₂/M mediates kidney fibrosis after injury. *Nat. Med.* **16**, 535–543, <https://doi.org/10.1038/nm.2144>
- 37 Johnson, A.C. and Zager, R.A. (2018) Plasma and urinary p21: potential biomarkers of AKI and renal aging. *Am. J. Physiol. Renal Physiol.* **315**, F1329–F1335, <https://doi.org/10.1152/ajprenal.00328.2018>
- 38 Bencokova, Z., Kaufmann, M.R., Pires, I.M., Lecane, P.S., Giaccia, A.J. and Hammond, E.M. (2009) ATM activation and signaling under hypoxic conditions. *Mol. Cell. Biol.* **29**, 526–537, <https://doi.org/10.1128/MCB.01301-08>
- 39 Tresini, M., Warmerdam, D.O., Kolovos, P., Snijder, L., Vrouwe, M.G., Demmers, J.A. et al. (2015) The core spliceosome as target and effector of non-canonical ATM signalling. *Nature* **523**, 53–58, <https://doi.org/10.1038/nature14512>
- 40 Baier, D., Teren, A., Wirkner, K., Loeffler, M. and Scholz, M. (2018) Parameters of pulse wave velocity: determinants and reference values assessed in the population-based study LIFE-Adult. *Clin. Res. Cardiol.* **107**, 1050–1061, <https://doi.org/10.1007/s00392-018-1278-3>
- 41 Otsuka, F., Yahagi, K., Sakakura, K. and Virmani, R. (2013) Why is the mammary artery so special and what protects it from atherosclerosis? *Ann. Cardiothorac. Surg.* **2**, 519–526
- 42 Guzik, T.J. and Touyz, R.M. (2017) Oxidative stress, inflammation, and vascular aging in hypertension. *Hypertension* **70**, 660–667, <https://doi.org/10.1161/HYPERTENSIONAHA.117.07802>
- 43 Wu, H. and Roks, A.J. (2014) Genomic instability and vascular aging: a focus on nucleotide excision repair. *Trends Cardiovasc. Med.* **24**, 61–68, <https://doi.org/10.1016/j.tcm.2013.06.005>
- 44 Said, M.A., Eppinga, R.N., Hagemeyer, Y., Verweij, N. and van der Harst, P. (2017) Telomere length and risk of cardiovascular disease and cancer. *J. Am. Coll. Cardiol.* **70**, 506–507, <https://doi.org/10.1016/j.jacc.2017.05.044>
- 45 Selfridge, J., Hsia, K.T., Redhead, N.J. and Melton, D.W. (2001) Correction of liver dysfunction in DNA repair-deficient mice with an ERCC1 transgene. *Nucleic Acids Res.* **29**, 4541–4550, <https://doi.org/10.1093/nar/29.22.4541>
- 46 Garinis, G.A., Uittenboogaard, L.M., Stachelscheid, H., Foustari, M., van Ijcken, W., Breit, T.M. et al. (2009) Persistent transcription-blocking DNA lesions trigger somatic growth attenuation associated with longevity. *Nat. Cell Biol.* **11**, 604–615, <https://doi.org/10.1038/ncb1866>
- 47 de Waard, M.C., van der Pluijm, I., Zuiderveen Borgesius, N., Comley, L.H., Haasdijk, E.D., Rijksen, Y. et al. (2010) Age-related motor neuron degeneration in DNA repair-deficient *Erc1* mice. *Acta Neuropathol.* **120**, 461–475, <https://doi.org/10.1007/s00401-010-0715-9>
- 48 Borgesius, N.Z., de Waard, M.C., van der Pluijm, I., Omrani, A., Zondag, G.C., van der Horst, G.T. et al. (2011) Accelerated age-related cognitive decline and neurodegeneration, caused by deficient DNA repair. *J. Neurosci.* **31**, 12543–12553, <https://doi.org/10.1523/JNEUROSCI.1589-11.2011>
- 49 Barnhoorn, S., Uittenboogaard, L.M., Jaarsma, D., Vermeij, W.P., Tresini, M., Weymaere, M. et al. (2014) Cell-autonomous progeroid changes in conditional mouse models for repair endonuclease XPG deficiency. *PLoS Genet.* **10**, e1004686, <https://doi.org/10.1371/journal.pgen.1004686>
- 50 Raj, D.D., Jaarsma, D., Holtman, I.R., Olah, M., Ferreira, F.M., Schaafsma, W. et al. (2014) Priming of microglia in a DNA-repair deficient model of accelerated aging. *Neurobiol. Aging* **35**, 2147–2160, <https://doi.org/10.1016/j.neurobiolaging.2014.03.025>
- 51 Bautista Nino, P.K., Durik, M., Danser, A.H., de Vries, R., Musterd-Bhaggoe, U.M., Meima, M.E. et al. (2015) Phosphodiesterase 1 regulation is a key mechanism in vascular aging. *Clin. Sci. (Lond.)* **129**, 1061–1075, <https://doi.org/10.1042/CS20140753>